Food crisis in Central Sahel in 2022 driven by chronic vulnerability with uncertain role of climate change

Audrey Brouillet[1], Benjamin Sultan[1], Clair Barnes[2], Mariam Zachariah[2], Friederike E. L. Otto[2], Maja Vahlberg [3], Roop Singh [3], Kiswendsida Guigma [3], Dorothy Heinrich [3], Cheikh Kane [3, 10], Maarten van Aalst [3], Lisa Thalheimer [8], Emmanuel Raju [9], Gerbrand Koren [4], Sjoukje Philip [5], Sarah Kew [5], Wenchang Yang [6], Robert Vautard [7]

[1] ESPACE-DEV, Univ Montpellier, IRD, Univ Guyane, Univ Reunion, Univ Antilles, Univ Avignon, Montpellier, France

[2] Grantham Institute, Imperial College London, United Kingdom

[3] Red Cross Red Crescent Climate Centre, The Hague, the Netherlands

[4] Copernicus Institute of Sustainable Development, Utrecht University, Utrecht, the Netherlands

[5] Royal Netherlands Meteorological Institute (KNMI), De Bilt, The Netherlands

[6] Department of Geosciences, Princeton University, Princeton, NJ 08544, USA

[7] Institut Pierre-Simon Laplace, CNRS, Sorbonne Université, Paris, France

[8] United Nations University, Institute for Environment and Human Security (UNU-EHS), Bonn, Germany

[9] Department of Public Health, Global Health Section & Copenhagen Centre for Disaster Research, University of Copenhagen, Denmark

[10] Institut de Recherche pour le Développement, U01000/99AA01, Marseille, France

Main findings are being edited here: websummary - West Africa drought

1 Introduction

At the beginning of the West Sahelian lean season in April-May 2022, alerts about food insecurity were raised in several countries of West Africa (Burkina Faso, Chad, Mali, Niger, Nigeria) (see e.g. NRC, 2022). This food shortage occurred after an erratic rainy season in summer 2021 which has affected crop production and reduced food stocks several months later. According to the Comité Permanent Inter-Etats de Lutte contre la Sécheresse dans le Sahel (CILSS) and its regional AGRHYMET institution, sowing dates were delayed by more than 15 days between June and July 2021 in south of Mauritania, central Mali, southern Niger and central Chad (mostly for millet and sorghum). CILSS also reported on severe water stress in these regions, with only less than 40% of crop water needs satisfied by 31 August 2021. Biomass loss in these regions compared to the previous 5 years was also estimated to be around -25 to -50% in the eastern part, and around -50 to -100% within the western part before 30 September 2021.

In this semi-arid region, the economy largely relies on rain-fed agriculture and pastoralism, and recurrently suffers from drought consequences. Although the region witnessed a multidecadal drought in the second half of the 20th century that was recovered in the subsequent better wet seasons, the region still suffers from episodic droughts. The rainy season is short (3-4 months between June and September) and dominated by monsoon convective episodes that can be intense but associated with patchy rainfall every year (e.g. LeBarbe et al., 2002; Laux et al., 2008). The lean season for this region coincides with the beginning of the new rainfall season. Therefore, delayed monsoon in any given year makes the population strongly dependent on the abundance (or the lack thereof) of the previous year's crop yield and other economic factors. This was the case for the year 2022, where the underlying issues due to poverty in the region were already inflated by other potential socio-economic drivers including the war in Ukraine, follow-up impacts of COVID on energy and crop prices, terrorism inducing population displacements and political unrest, and was likely aggravated further by the short rainy season and the delayed rainfall onset in the preceding year, 2021.

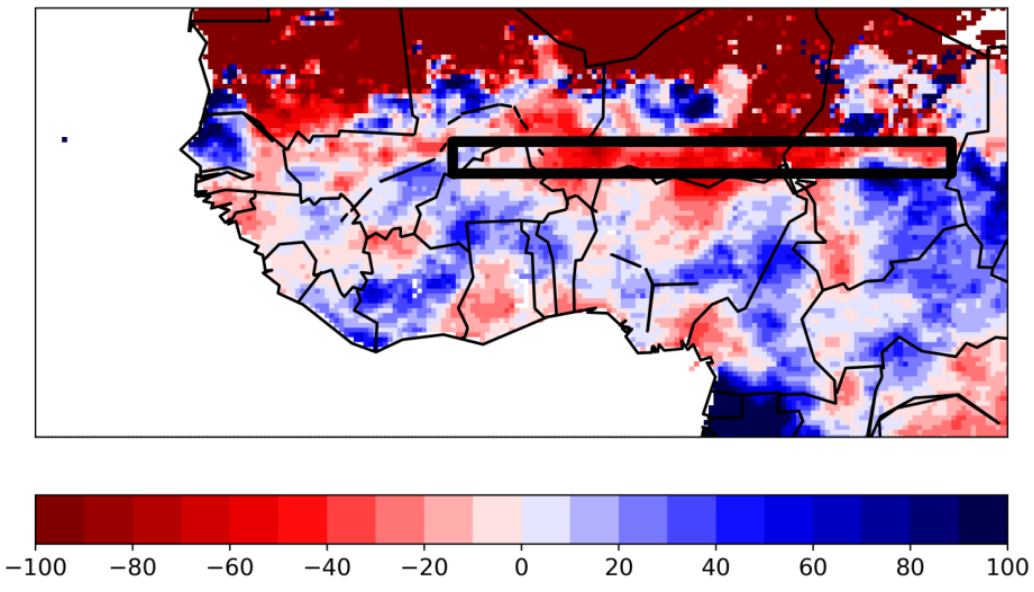

***Figure 1**: Spatial distribution of anomalies of precipitation amount in June in 2021 for CHIRPS dataset (in % relative to average June precipitation over 1990-2020) over part of Western and Central Africa. The black rectangle indicates the study domain.*

1.1 The meteorological event

Figure 1 shows the normalised anomaly of June 2021 precipitation amount relative to a 1990-2020 climatology, based on the Climate Hazards Group InfraRed Precipitation with Station data (CHIRPS) dataset (Funk et al., 2015; Sacré et al., 2020). While the pattern is patchy as expected, there is a wide band of negative anomaly as strong as -50%, from Mali through South Niger till central Chad (highlighted by the black box in Figure 1), which are densely populated, agrarian regions, unlike the largely desertic northern regions. Although this deficit was followed by an excess of rainfall in July, there was again a strong deficit in September, thus making the wet season very short in these countries.

Rainfall deficits in the beginning of the rainy season and again in September have the potential to strongly impact crop production and food security. Staple crops are mainly rain-fed in the Sahel-crop cycles of millet and sorghum coincide with the summer rainy season that is also the unique source of water for these crops. Therefore, immediate dry spells following the sowing period of these crops at the beginning of the rainy season can spoil the seeds, thus compromising the development of the crop (Marteau et al., 2011).

Dry spells in September can also have a strong impact on crop yields as they coincide with the most water-sensitive development stages of the crop, i.e. the flowering and grain-ripening stages (Sultan et al., 2005). The Regional Center AGRHYMET estimated that crops experienced a severe water stress in Central Mali, Southern Niger and Chad with a delayed sowing date of more than 20 days and less than 40% of their water needs satisfied (Cadre Harmonisé). It affected cereal production, contributing to driving up prices of food and agricultural inputs. Niger and Burkina Faso recorded reductions in cereal production of 36% and 10% compared with the previous five-year average, respectively. In Burkina Faso, maize prices increased by 50% compared to the five-year average, while in Niger, the price of sorghum was 40% above the five-year average and the price of millet increased by 30% (Cadre Harmonisé; World Meteorological Organization, 2022). The situation was worsened by population displacement resulted from security incidents and jihadist insurgency.

When such an anomalous situation occurs, climate change is often invoked as fostering the intensity, frequency or other characteristics of the event. The IPCC report (IPCC, 2021: Chapter 12) states that there is *low confidence* that precipitation will increase in Central and Eastern Sahel for global warming levels of 1.5°C and 2°C relative to recent past, and in West Africa there is *low confidence* of an increase in agro-ecological droughts so far attributable to climate change (IPCC, 2021: Chapter 11). Also, a change in seasonality has been reported, with later onsets and ends of the monsoon season (see also IPCC, 2021: Chapter 8). The region therefore needs more studies to assess the influence of climate change on the rainy season.

1.2 Event definition

According to the above anomalies, we choose to focus on precipitation indicators to emphasise the alerted dry event, with several indicators characterising anomalies of the rainy season of 2021, based on the above analysis. The corresponding rainy season features can thus define the event, i.e. later

rainy season start (onset), shorter duration, less amount of rain (over the total rainy season or the starting month, i.e. June).

To calculate the rainy season onset (and corresponding demise and duration), we use the method of Liebmann and Marengo (2001), described in Bombardi et al., (2019). The method uses the accumulated precipitation anomalies $S_{t,y} = \sum_{t0:t}\left(p_{t,y} - \overline{p}_{y}\right)$, where y is the current year; t is the day of the year; $t0$ is start of the current year; $p_{t,y}$ is the daily precipitation rate on day t of year y; and $\overline{p}$ is the mean daily precipitation in year y. The daily accumulated anomalies are smoothed using a 15-day moving window centered on day i, and the rainy season for year y is defined as the longest consecutive period in year y when this smoothed difference in daily accumulated anomalies is greater than zero, with the onset date taken as the first day in this period, and the duration date as the last day in this period. Strictly speaking, $t0$ denotes the midpoint of the dry season, which falls in mid-February according to the observed seasonal cycle: however, as Bombardi et al. (2019) noted, for regions that experience well-defined rainy seasons – as is the case here – the date of inflection of accumulated precipitation anomalies does not depend on the "beginning" of the accumulated precipitation anomaly calculation (i.e. $t0$), and so $t0$ is set to the start of the calendar year. The method can be somewhat sensitive to the choice of the smoothing parameter, which determines whether shorter periods of rainfall are merged with the unbroken rainy season: however, similar results were obtained when using a window of between 7 and 21 days.

We average time series over the Central Sahel region covering the June precipitation anomaly [3°W,24°E ; 14°N,16°N] region/box, shown in Figure 1. As a summary, we use 3 indices along this study, calculated as specified above:

1. The precipitation amount in June.
2. The monsoon onset date.
3. The rainy season duration.

2 Data and methods

2.1 Observational data

Availability of long-term, homogeneous, meteorological station data in Africa is a strong limitation in such a study since time series using satellite retrievals are short for proper assessment of return periods of extreme events and since the quality of satellite rainfall products could be affected by the very low number of stations used for estimating rainfall. The World Meteorological Organization (2020) estimated that in 2019, only 26% of African GCOS GSN stations (Global Climate Observing System Surface Network) reported according to the agreed WMO requirements, a trend which has not changed since 2011, with 35% of the stations non-operational (WMO, 2020). With that in mind and based on precipitation dataset comparison studies over the region (Beck et al., 2017; Satgé et al., 2020), we use three gridded datasets for fitting probability distributions to rainfall in the study domains and thereafter to analyze the dry episode event of 2021 in West Africa in the context of climate change.

The first analyzed dataset is the Climate Hazards Group InfraRed Precipitation with Station data (CHIRPS) and corresponds to a 35+ year quasi-global rainfall data set (Funk et al. 2015, Sacré et al. 2020). Spanning 50°S-50°N (and all longitudes) and ranging from 1981 to near-present, CHIRPS incorporates climatology, CHPclim, 0.05° resolution satellite imagery, and in-situ station data to create gridded rainfall time series for trend analysis and seasonal drought monitoring. The second analyzed dataset is the Tropical Applications of Meteorology using SATellite data and ground-based observations (TAMSAT), which produces daily rainfall estimates for all of Africa at 4 km resolution from 1983 to near present (Tarnavsky et al. 2014, Maidment et al. 2017). Finally, we analyse the Multi-Source Weighted-Ensemble Precipitation (MSWEP), which is a global precipitation product with a 3-hourly 0.1° resolution available from 1979 to now (Beck et al., 2019). MSWEP (version v2.8) incorporates daily gauge observations and accounts for gauge reporting times to reduce temporal mismatches between satellite-reanalysis estimates and gauge observations. The last few points are from the near real time (NRT) version and could be different from the final release.

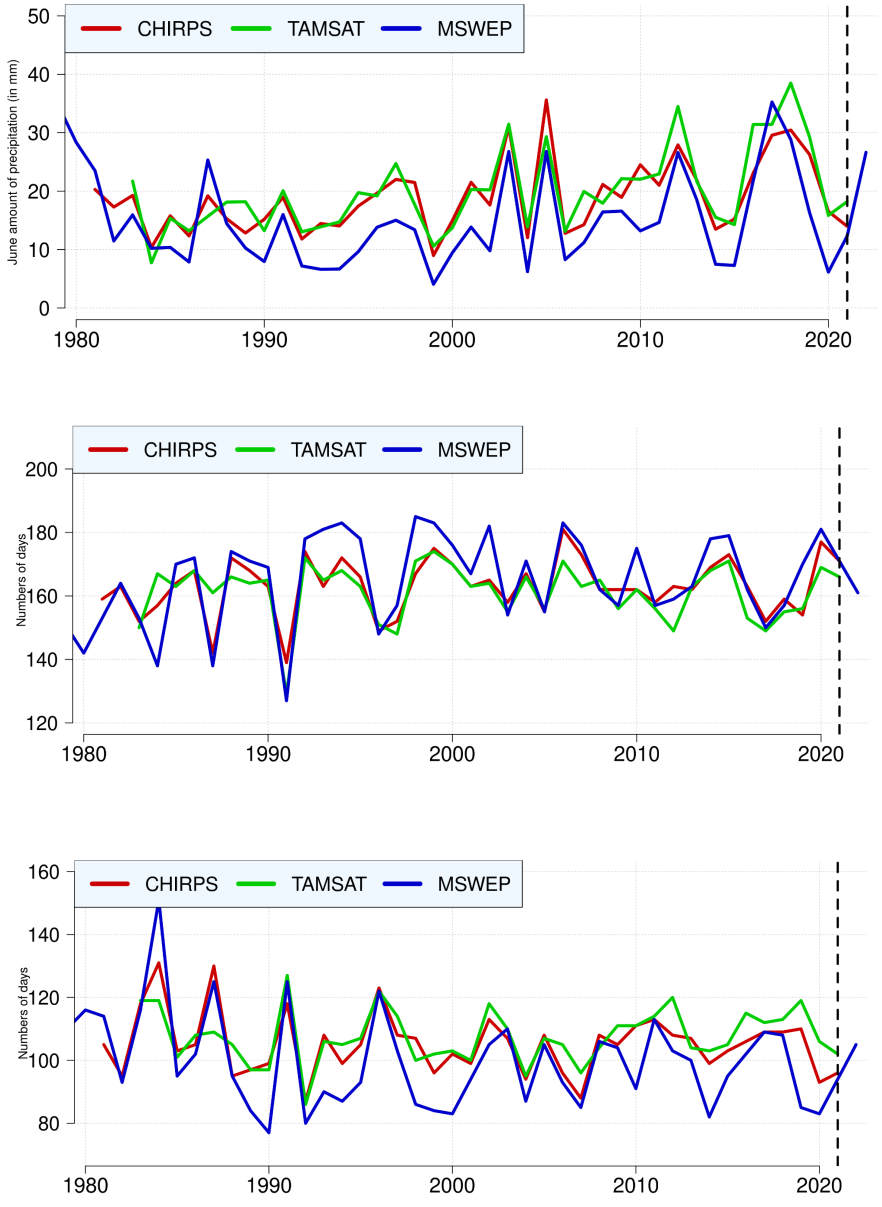

Figure 2 : Top panel: Time series of total June precipitation and comparison of the three datasets used in this study averaged over central Sahel. Note that the CHIRPS dataset covers 1981-2021, TAMSAT covers 1983-2021 and MSWEP covers 1979-2022. Middle and bottom panels: Same as top panel but for the onset date and the rainy season duration.

Figure 2a-c shows time series of total June total precipitation, rainy season onset dates and rainy season duration respectively, all averaged over Central Sahel and for the three gridded datasets analysed in the present study. In general, all three gridded datasets are found to match the observed variability in the station-based averages, particularly for total June precipitation and rainy season onsets. However, rainy season duration shows larger discrepancies, particularly for MSWEP in comparison to CHIRPS and TAMSAT. Moreover, MSWEP displays an increasing (decreasing) trend for rainy season onsets (durations) that is not that significant using CHIRPS nor TAMSAT datasets. Due to inconsistencies among the three datasets in length, trends and the magnitude of the 2021 event and for the three selected indicators, and no reason to select one dataset over another, we use all three datasets for evaluating the observed trends and return times that are subsequently used for climate model evaluation (discussed in Section 4).

Finally, and as a measure of anthropogenic climate change, we use the (low-pass filtered) global mean surface temperature (GMST), where GMST is taken from the National Aeronautics and Space Administration (NASA) Goddard Institute for Space Science (GISS) surface temperature analysis (GISTEMP; Hansen et al., 2010, Lenssen et al., 2019).

2.2 Model and experiment descriptions

CMIP6

The Coupled Model Intercomparison Project (CMIP) organised under the auspices of the World Climate Research Programme's (WCRP) Working Group on Coupled Modelling (WGCM) started 20 years ago and currently provides a comparison of a handful of global coupled climate models through the 6th phase of CMIP (CMIP6; Eyring et al. 2016). In the present study we analyse a set of 0.5° spatial resolution 21 CMIP6 models for the period 1950-2100, both under the *historical* scenario (1950-2014) and under the strong emissive future Shared Socioeconomic Pathways *ssp585* scenario (2015 until 2050 or 2100 depending on the model; Eyring et al. 2016, Kriegler et al. 2017, Riahi et al. 2017). These data are bias-corrected using the CDF-t method conducted in Famien et al. (2018).

HighResMIP

We also use the HighResMIP SST-forced model ensemble (Haarsma et al. 2016), the simulations for which span from 1950 to 2050. The SST and sea ice forcings for the period 1950-2014 are obtained from the 0.25° x 0.25° Hadley Centre Global Sea Ice and Sea Surface Temperature dataset that are area-weighted regridded to match the climate model resolution. For the 'future' time period (2015-2050), SST/sea-ice data are derived from RCP8.5 (CMIP5) data, and combined with greenhouse gas forcings from SSP5-8.5 (CMIP6) simulations (see Section 3.3 of Haarsma et al. 2016 for further details).

CORDEX-Africa and CORDEX-CORE

CORDEX-Africa (0.44° resolution, AFR-44) is a multi-model ensemble (Nikulin et al., 2012) covering the whole of Africa. The ensemble used here consists of 16 simulations resulting from pairings (as of November 2021) of Global Climate Models (GCMs) and Regional Climate Models (RCMs) (see the table below). These simulations are composed of historical simulations up to 2005 and then extended to the end of the 21th century using the RCP8.5 scenario. For each simulation, we consider the entire period available for attribution (until 2022). All models were tested for the Gaussian parameters against observations. CORDEX-CORE experiments covering Africa (0.22° resolution, AFR-22) are also used here.

AM2.5C360 and FLOR

The models used in the analysis also include the FLOR (Vecchi et al., 2014) high-resolution climate models developed at Geophysical Fluid Dynamics Laboratory (GFDL) and the AM2.5C360 (Yang et al., 2021; Chan et al., 2021). The FLOR model is an atmosphere-ocean coupled GCM with a resolution of 50 km for land and atmosphere and 1 degree for ocean and ice. Ten ensemble simulations from FLOR are analysed, which cover the period from 1860 to 2100 and include both the historical and RCP4.5 experiments driven by transient radiative forcings from CMIP5 (Taylor et al., 2012). The AM2.5C360, on the other hand, is an atmospheric GCM based on that in the FLOR model (Delworth et al., 2012; Vecchi et al., 2014) with a horizontal resolution of 25 km. Three ensemble simulations of the Atmospheric Model Intercomparison Project (AMIP) experiment from 1871 to 2050 are analysed. These simulations are initialised from three different pre-industrial conditions but forced by the same SSTs from HadISST1 (Rayner et al., 2003) after groupwise adjustments (Chan et al., 2021) over the period of 1871-2020. The SSTs from 2021 to 2050 are from the FLOR simulations after climatology bias correction based on HadISST1.

2.3 Statistical methods

In this analysis we examine mean rainfall data in June, averaged over the Central Sahel band (as defined in Section 1), as well as two other indices characterizing the rainy season of 2021. Methods for observational and model analysis and for model evaluation and synthesis are used according to the World Weather Attribution Protocol, described in Philip et al. (2020), with supporting details found in van Oldenborgh et al. (2021), Ciavarella et al. (2021) and here.

The analysis steps include: (i) trend calculation from observations; (ii) model evaluation; (iii) multi-method multi-model attribution and (iv) synthesis of the attribution statement.
We calculate the return periods, Probability Ratio and change in intensity of the event in question when comparing observed GMST values of 2021 with past GMST values (1850-1900, based on the Global Warming Index https://www.globalwarmingindex.org), an estimated difference of 1.2°C.

To statistically model the event in question, we tested the Generalized Pareto Distribution (GPD) that scales with GMST, for the June precipitation, as for our study over Madagascar (Harrington et al., 2021), but the amount of data was insufficient, and finally opted for a simpler, Gaussian, distribution, with sigma-over-mu scaling with the GMST. For the onset date and rainy season length, we also opted for a Gaussian distribution fit, with a shift of location parameter assumed.

Finally, results from observations and models that pass the validation tests (see Section 4) are synthesized into a single attribution statement, in the standard manner.

3 Observational analysis: return time and trend

Fig. 3 left panels show the response of the total June precipitation amount to the global mean temperature over Central Sahel. Right panels in Fig. 3 show the return period curves in the present 2021 climate and the past climate when the global mean temperature was 1.2 °C cooler. We find that the return period of the total June precipitation in the 2021 climate is consistent across CHIRPS and TAMSAT datasets (ranging from 0-20 years), but is different in MSWEP dataset (2-4 years). We round this to 10 years for the remainder of the analysis for this indicator.

Similar plots for the rainy season onset (start) are shown in Fig. 4. The return periods of this event in the current 2021 climate are found to closely match in TAMSAT and MSWEP but less in CHIRPS (right panels in Fig. 4). The return period is here rounded to 3 years for this onset indicator for the rest of the analysis.

Fig. 5 shows the same plots for the rainy season duration index. The return periods of this event in the current 2021 climate closely match in the three datasets, and the return period is here rounded to 3 years for this onset indicator for the rest of the analysis.

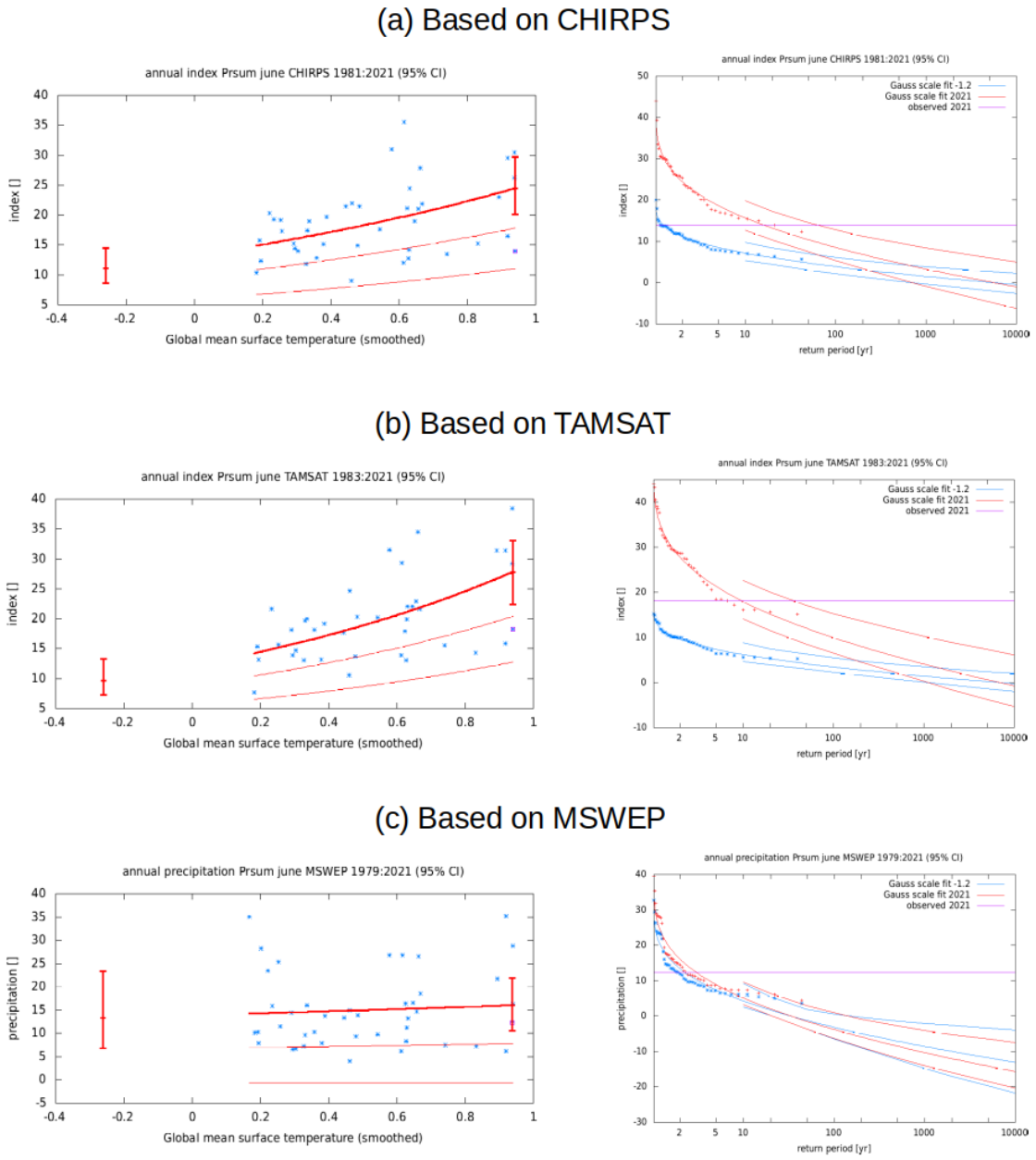

Figure 3: Gaussian fit with constant dispersion parameters, and location parameter scaling proportional to GMST of the index series, for the **total June precipitation** based on three gridded datasets- (a) CHIRPS (b) TAMSAT and (c) MSWEP. The 2021 event is included in the fit. Left: Total June precipitation (in mm) as a function of the smoothed GMST. The thick red line denotes the time-varying location parameter. The vertical red lines show the 95% confidence interval for the location parameter, for the current, 2021 climate and a 1.2ºC cooler climate. The 2021 observation is highlighted with the magenta box. Right: Return time plots for the climate of 2021 (red) and a climate with GMST 1.2 ºC cooler (blue). The past observations are shown twice: once scaled to the current climate and once scaled to the climate of the late nineteenth century. The markers show the data and the lines show the fits and uncertainty from the bootstrap. The magenta line shows the magnitude of the 2021 event analysed here.

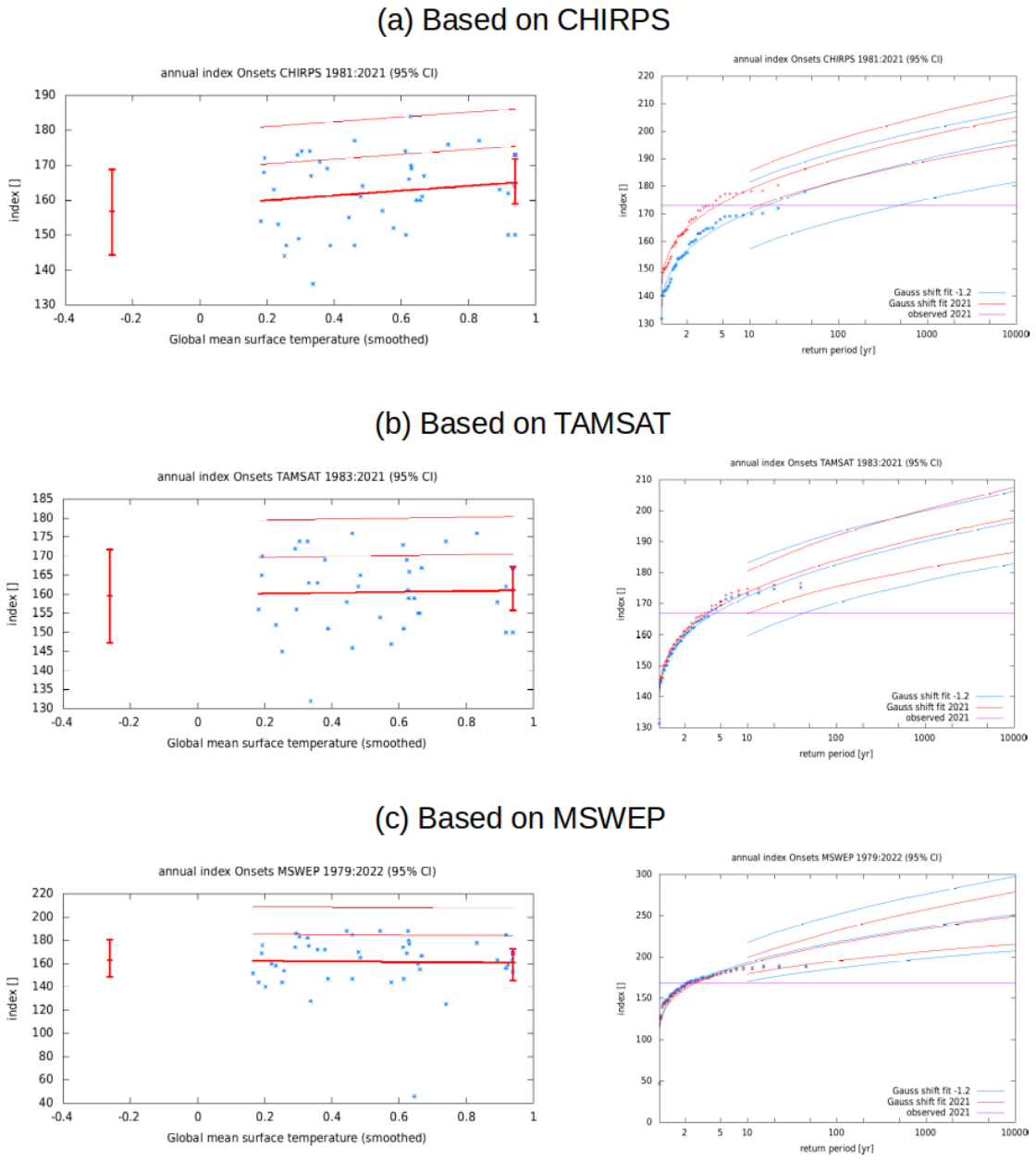

Figure 4: Gaussian fit with constant dispersion parameters, and location parameter shifting proportional to GMST of the index series, for the **rainy season onset** based on three gridded datasets- (a) CHIRPS (b) TAMSAT and (c) MSWEP. The 2021 event is included in the fit. Left: Rainy season onset (in day of the year) as a function of the smoothed GMST. The thick red line denotes the time-varying location parameter. The vertical red lines show the 95% confidence interval for the location parameter, for the current, 2021 climate and a 1.2ºC cooler climate. The 2021 observation is highlighted with the magenta box. Right: Return time plots for the climate of 2021 (red) and a climate with GMST 1.2 ºC cooler (blue). The past observations are shown twice: once shifted to the current climate and once shifted to the climate of the late nineteenth century. The markers show the data and the lines show the fits and uncertainty from the bootstrap. The magenta line shows the magnitude of the 2021 event analysed here.

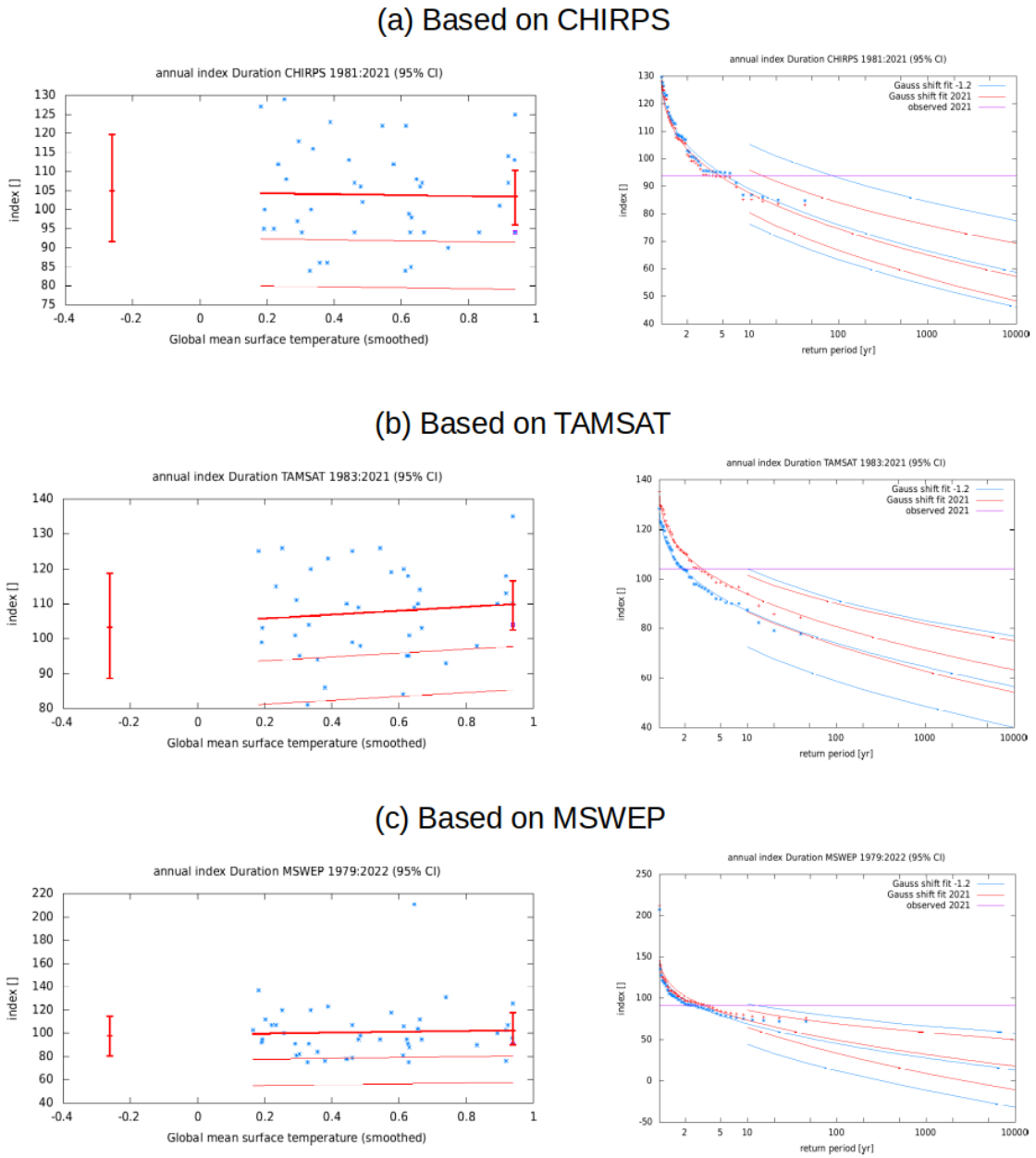

Figure 5: Gaussian fit with constant dispersion parameters, and location parameter shifting proportional to GMST of the index series, for the **rainy season duration** based on three gridded datasets- (a) CHIRPS (b) TAMSAT and (c) MSWEP. The 2021 event is included in the fit. Left: Rainy season duration (in number of days) as a function of the smoothed GMST. The thick red line denotes the time-varying location parameter. The vertical red lines show the 95% confidence interval for the location parameter, for the current, 2021 climate and a 1.2ºC cooler climate. The 2021 observation is highlighted with the magenta box. Right: Return time plots for the climate of 2021 (red) and a climate with GMST 1.2 ºC cooler (blue). The past observations are shown twice: once shifted to the current climate and once shifted to the climate of the late nineteenth century. The markers show the data and the lines show the fits and uncertainty from the bootstrap. The magenta line shows the magnitude of the 2021 event analysed here.

4 Model evaluation

In the subsections below we show the results of the model evaluation for the two event definitions. Per framing or model setup we use both the good and reasonable models. The tables show the model evaluation results. The model evaluation and selection is carried out by verifying the following elements:

- Satisfactory seasonal cycles for the index used (here, rainfall averaged over Central Sahel), with an emphasis on capturing the monsoon peak in the right months (from June to August);
- Satisfactory spatial patterns of mean rainfall during the central monsoon months (June to August)
- Model fit parameter (dispersion and shape) confidence intervals that overlap with those from observations.

***Table 1**: Evaluation results for the climate models considered for the attribution analysis of the mean precipitation in the month of June, for the study region. The table contains qualitative assessments of seasonal cycle and spatial pattern of precipitation from the models (good, reasonable, bad) along with estimates for dispersion parameter, and event magnitude. The corresponding estimates for the observed datasets are shown in blue. Based on overall suitability, the models are classified as good, reasonable and bad, shown by green, yellow and red highlights, respectively. <n.e> stands for not estimated.*

Observations	**Seasonal cycle**	**Spatial pattern**	**June precipitation**	
			Dispersion	**Event magnitude (mm/day)**
CHIRPS			-0.280 (-0.335 ... -0.216)	14
TAMSAT			-0.276 (-0.322 ... -0.215)	18.2
MSWEP			-0.474 (-0.537 ... -0.367)	2.1
Model				**Threshold for 10-yr return period**
ACCESS-CM2_historical-ssp585	reasonable	reasonable	-0.523 (-0.655 ... -0.315)	14.25
ACCESS-ESM1-5_historical-ssp585	bad	reasonable	-0.689 (-0.804 ... -0.452)	<n.e>
BCC-CSM2-MR_historical-ssp585	reasonable	reasonable	-0.375 (-0.424 ... -0.300)	36.22
CanESM5_historical-ssp585	bad	reasonable	<n.e>	<n.e>
CNRM-CM6-1_historical-ssp585	good	reasonable	-0.511 (-0.574 ... -0.415)	<n.e>
CNRM-CM6-1-HR_historical-ssp585	reasonable	reasonable	-0.425 (-0.513 ... -0.281)	12.75
CNRM-ESM2-1_historical-ssp585	good	reasonable	-0.483 (-0.571 ... -0.343)	<n.e>
GFDL-CM4_historical-ssp585	reasonable	reasonable	-0.461 (-0.534 ... -0.352)	<n.e>
INM-CM5-0_historical-ssp585	bad	reasonable	<n.e>	<n.e>
IPSL-CM6A-LR_historical-ssp585	good	reasonable	-0.468 (-0.559 ... -0.327)	12.83
KACE-1-0-G_historical-ssp585	bad	bad	<n.e>	<n.e>

MIROC6_historical-ssp585	good	reasonable	-0.584 (-0.701 ... -0.418)	<n.e>
MIROC-ES2L_historical-ssp585	good	reasonable	-0.694 (-0.796 ... -0.559)	<n.e>
MPI-ESM1-2-LR_historical-ssp585	reasonable	reasonable	-0.377 (-0.441 ... -0.215)	15.14
MRI-ESM2-0_historical-ssp585	bad	reasonable	<n.e>	<n.e>
NESM3_historical-ssp585	bad	reasonable	<n.e>	<n.e>
NorESM2-LM_historical-ssp585	good	reasonable	-0.600 (-0.713 ... -0.378)	<n.e>
NorESM2-MM_historical-ssp585	reasonable	reasonable	-0.502 (-0.568 ... -0.391)	<n.e>
UKESM1-0-LL_historical-ssp585	bad	bad	<n.e>	<n.e>
EC-EARTH3P	bad	good	-0.863 (-1.04 ... -0.658)	-0.53
EC-EARTH3P-HR	reasonable	reasonable	-0.989 (-1.14 ... -0.708)	-1.99
HADGEM3-GC31-LM	reasonable	good	-0.515 (-0.598 ... -0.389)	7.48
HADGEM3-GC31-MM	reasonable	good	-0.416 (-0.471 ... -0.317)	15.23
HADGEM3-GC31-HM	reasonable	good	-0.407 (-0.463 ... -0.315)	12.35
CMCC-CM2-HR4	reasonable	good	-0.328 (-0.378 ... -0.263)	29.56
CMCC-CM2-VHR4	reasonable	good	-0.341 (-0.418 ... -0.243)	37.5
CNRM-CM6-1	reasonable	good	-1.16 (-1.32 ... -0.868)	-13.58
MPI-ESM1-2-HR	bad	good	-1.52 (-1.70 ... -0.693)	-3.01
MPI-ESM1-2-XR	bad	good	-0.935 (-1.10 ... -0.713)	-1.1
AM2.5C360	good	good	-0.336 (-0.375 ... -0.287)	33.6
FLOR	bad	reasonable	-0.496 (-0.532 ... -0.457)	19.63
CanESM2-CanRCM4	bad	bad	-0.138 (-0.159 ... -0.110)	71.79
CNRM-CM5_r1i1p1_CCLM4-8-17	reasonable	reasonable	-0.280 (-0.331 ... -0.214)	77.02
EC-EARTH_r12i1p1_CCLM4-8-17	bad	good	-0.456 (-0.524 ... -0.368)	44.15
EC-EARTH_r12i1p1_RACMO22T	bad	reasonable	-0.667 (-0.787 ... -0.470)	9.05
EC-EARTH_r12i1p1_REMO2009	bad	good	-0.468 (-0.527 ... -0.382)	7.25
EC-EARTH_r1i1p1_RACMO22T	bad	reasonable	-0.525 (-0.611 ... -0.374)	8.43
EC-EARTH_r3i1p1_HIRHAM5	reasonable	good	-0.643 (-0.742 ... -0.462)	8.71
IPSL-CM5A-LR_r1i1p1_REMO2009	good	good	-0.678 (-0.784 ... -0.532)	1.08
MIROC5_r1i1p1_REMO2009	good	good	-0.603 (-0.723 ... -0.420)	4.79
HadGEM2-ES_r1i1p1_CCLM4-8-17	bad	good	-0.456 (-0.516 ... -0.365)	45.97
HadGEM2-ES_r1i1p1_REMO2009	good	good	-0.500 (-0.578 ... -0.385)	11.72
HadGEM2-ES_r1i1p1_RACMO22T	bad	reasonable	-0.569 (-0.689 ... -0.443)	15.42
MPI-ESM-LR_r1i1p1_CCLM4-8-17	reasonable	good	-0.532 (-0.614 ... -0.414)	27.97

MPI-ESM-LR_r1i1p1_REMO2009	good	good	-0.465 (-0.536 ... -0.360)	5.09
MPI-ESM-MR_r1i1p1_RegCM4-3	bad	good	-0.640 (-0.767 ... -0.449)	0.00008
GFDL-ESM2G_r1i1p1_REMO2009	good	good	-0.531 (-0.628 ... -0.364)	4.00
HadGEM2-ES_r1i1p1_CCLM5-0-15	reasonable	bad	-0.386 (-0.457 ... -0.304)	47.28
HadGEM2-ES_r1i1p1_REMO2015	good	good	-0.483 (-0.553 ... -0.380)	11.47
HadGEM2-ES_r1i1p1_RegCM4-7	reasonable	good	-1.10 (-1.30 ... -0.825)	-26.37
MPI-ESM-LR_r1i1p1_CCLM5-0-15	good	good	-0.638 (-0.738 ... -0.513)	10.64
MPI-ESM-LR_r1i1p1_REMO2015	good	good	-0.556 (-0.658 ... -0.398)	5.32
MPI-ESM-MR_r1i1p1_RegCM4-7	bad	good	-1.68 (-2.14 ... -1.23)	-5.73
NorESM1-M_r1i1p1_CCLM5-0-15	bad	good	-0.463 (-0.555 ... -0.354)	32.04
NorESM1-M_r1i1p1_REMO2015	reasonable	good	-0.526 (-0.610 ... -0.414)	5.48
NorESM1-M_r1i1p1_RegCM4-7	bad	good	-1.39 (-1.66 ... -1.05)	-12.01

***Table 2**: same as Table 1, for the rainy season onset.*

			Rainy season onset	
Observations	**Seasonal cycle**	**Spatial pattern**	**Sigma**	**Event magnitude (day of the year)**
CHIRPS			10.8 (8.73 ... 12.4)	173
TAMSAT			9.87 (7.51 ... 11.7)	167
MSWEP			23.8 (13.3 ... 34.0)	169
Model				**Threshold for 3-yr return period**
ACCESS-CM2_historical-ssp585	reasonable	reasonable	13.2 (10.5 ... 15.1)	177.3
ACCESS-ESM1-5_historical-ssp585	bad	reasonable	13.2 (10.4 ... 14.9)	<n.e>
BCC-CSM2-MR_historical-ssp585	reasonable	reasonable	10.3 (7.19 ... 12.7)	136.27
CanESM5_historical-ssp585	bad	reasonable	13.4 (10.6 ... 15.4)	<n.e>
CNRM-CM6-1_historical-ssp585	good	reasonable	17.0 (13.3 ... 19.7)	<n.e>
CNRM-CM6-1-HR_historical-ssp585	reasonable	reasonable	15.5 (9.93 ... 20.3)	168.17
CNRM-ESM2-1_historical-ssp585	good	reasonable	17.9 (14.2 ... 20.0)	<n.e>
GFDL-CM4_historical-ssp585	reasonable	reasonable	16.7 (13.2 ... 19.1)	<n.e>
INM-CM5-0_historical-ssp585	bad	reasonable	9.07 (6.09 ... 11.5)	<n.e>
IPSL-CM6A-LR_historical-ssp585	good	reasonable	14.5 (10.5 ... 17.6)	161.89
KACE-1-0-G_historical-ssp585	bad	bad	71.2 (54.8 ... 81.2)	<n.e>
MIROC6_historical-ssp585	good	reasonable	14.2 (11.0 ... 16.2)	165.32
MIROC-ES2L_historical-ssp585	good	reasonable	16.9 (12.5 ... 20.2)	<n.e>

MPI-ESM1-2-LR_historical-ssp585	reasonable	reasonable	15.9 (11.7 ... 18.9)	163.77
MRI-ESM2-0_historical-ssp585	bad	reasonable	13.9 (11.2 ... 15.9)	<n.e>
NESM3_historical-ssp585	bad	reasonable	16.9 (11.8 ... 20.8)	<n.e>
NorESM2-LM_historical-ssp585	good	reasonable	17.4 (14.1 ... 19.6)	<n.e>
NorESM2-MM_historical-ssp585	reasonable	reasonable	16.2 (12.1 ... 19.1)	<n.e>
UKESM1-0-LL_historical-ssp585	bad	bad	69.0 (54.2 ... 79.8)	<n.e>
EC-EARTH3P	bad	good	7.59 (6.05 ... 8.68)	187.09
EC-EARTH3P-HR	reasonable	reasonable	6.03 (4.43 ... 7.30)	185.61
HADGEM3-GC31-LM	reasonable	good	18.8 (14.0 ... 22.4)	167.02
HADGEM3-GC31-MM	reasonable	good	19.8 (16.4 ... 21.9)	164.54
HADGEM3-GC31-HM	reasonable	good	17.9 (13.7 ... 21.1)	169.71
CMCC-CM2-HR4	reasonable	good	17.8 (11.9 ... 21.4)	172.67
CMCC-CM2-VHR4	reasonable	good	15.1 (11.9 ... 17.2)	169.91
CNRM-CM6-1	reasonable	good	31.0 (24.3 ... 35.3)	210.37
MPI-ESM1-2-HR	bad	good	6.87 (4.52 ... 8.79)	189.71
MPI-ESM1-2-XR	bad	good	5.60 (4.58 ... 6.21)	188.1
AM2.5C360	good	good	16.6 (14.6 ... 18.3)	160.28
FLOR	bad	reasonable	27.5 (26.1 ... 28.9)	178.44
CanESM2-CanRCM4	bad	bad	14.0 (9.41 ... 17.8)	117.45
CNRM-CM5_r1i1p1_CCLM4-8-17	reasonable	reasonable	18.4 (13.8 ... 22.3)	170.44
EC-EARTH_r12i1p1_CCLM4-8-17	bad	good	22.3 (17.4 ... 25.3)	176.55
EC-EARTH_r12i1p1_RACMO22T	bad	reasonable	27.0 (7.45 ... 37.0)	217.17
EC-EARTH_r12i1p1_REMO2009	bad	good	18.9 (13.7 ... 22.3)	182.59
EC-EARTH_r1i1p1_RACMO22T	bad	reasonable	25.8 (17.1 ... 31.6)	193.98
EC-EARTH_r3i1p1_HIRHAM5	reasonable	good	12.5 (9.23 ... 14.6)	187.46
IPSL-CM5A-LR_r1i1p1_REMO2009	good	good	10.6 (8.63 ... 12.1)	183.61
MIROC5_r1i1p1_REMO2009	good	good	9.62 (7.03 ... 11.7)	188.75
HadGEM2-ES_r1i1p1_CCLM4-8-17	bad	good	14.7 (10.5 ... 17.2)	168.28
HadGEM2-ES_r1i1p1_REMO2009	good	good	12.1 (9.22 ... 14.3)	179.46
HadGEM2-ES_r1i1p1_RegCM4-3	bad	good	15.5 (11.6 ... 18.0)	174.43
HadGEM2-ES_r1i1p1_RACMO22T	bad	reasonable	23.9 (18.2 ... 28.4)	181.62
MPI-ESM-LR_r1i1p1_CCLM4-8-17	reasonable	good	19.3 (14.8 ... 22.6)	191.96
MPI-ESM-LR_r1i1p1_REMO2009	good	good	13.1 (9.87 ... 15.5)	187.66

MPI-ESM-MR_r1i1p1_RegCM4-3	bad	good	26.4 (19.9 ... 30.6)	191.38
GFDL-ESM2G_r1i1p1_REMO2009	good	good	17.6 (12.3 ... 21.1)	186.87
HadGEM2-ES_r1i1p1_CCLM5-0-15	reasonable	bad	11.9 (7.65 ... 15.3)	169.63
HadGEM2-ES_r1i1p1_REMO2015	good	good	8.94 (6.72 ... 10.6)	174.2
HadGEM2-ES_r1i1p1_RegCM4-7	reasonable	good	17.6 (9.48 ... 23.4)	194.56
MPI-ESM-LR_r1i1p1_CCLM5-0-15	good	good	17.4 (13.9 ... 19.6)	193.46
MPI-ESM-LR_r1i1p1_REMO2015	good	good	14.9 (10.2 ... 18.4)	181.93
MPI-ESM-MR_r1i1p1_RegCM4-7	bad	good	12.0 (8.49 ... 14.4)	212.34
NorESM1-M_r1i1p1_CCLM5-0-15	bad	good	20.1 (15.8 ... 23.0)	173.42
NorESM1-M_r1i1p1_REMO2015	reasonable	good	25.5 (21.1 ... 28.0)	175.64
NorESM1-M_r1i1p1_RegCM4-7	bad	good	36.0 (27.0 ... 41.2)	202.58

***Table Z**: same as Table X, for the rainy season duration.*

Observations	**Seasonal cycle**	**Spatial pattern**	**Rainy season duration**	
			Sigma	**Event magnitude (days)**
CHIRPS			12.4 (9.91 ... 14.0)	94
TAMSAT			12.5 (9.88 ... 14.5)	104
MSWEP			22.8 (12.8 ... 32.7)	91
Model				**Threshold for 3-yr return period**
ACCESS-CM2_historical-ssp585	reasonable	reasonable	15.4 (11.9 ... 17.8)	107.69
ACCESS-ESM1-5_historical-ssp585	bad	reasonable	17.3 (12.3 ... 21.3)	<n.e>
BCC-CSM2-MR_historical-ssp585	reasonable	reasonable	12.9 (9.95 ... 15.1)	111.98
CanESM5_historical-ssp585	bad	reasonable	15.2 (11.9 ... 17.5)	<n.e>
CNRM-CM6-1_historical-ssp585	good	reasonable	17.1 (14.6 ... 18.9)	<n.e>
CNRM-CM6-1-HR_historical-ssp585	reasonable	reasonable	19.8 (13.4 ... 24.4)	<n.e>
CNRM-ESM2-1_historical-ssp585	good	reasonable	20.5 (15.5 ... 24.4)	<n.e>
GFDL-CM4_historical-ssp585	reasonable	reasonable	17.0 (12.6 ... 20.3)	<n.e>
INM-CM5-0_historical-ssp585	bad	reasonable	12.2 (8.94 ... 15.2)	<n.e>
IPSL-CM6A-LR_historical-ssp585	good	reasonable	15.3 (11.2 ... 18.5)	108.89
KACE-1-0-G_historical-ssp585	bad	bad	74.1 (53.5 ... 90.1)	<n.e>
MIROC6_historical-ssp585	good	reasonable	17.2 (13.8 ... 19.4)	<n.e>
MIROC-ES2L_historical-ssp585	good	reasonable	18.9 (14.2 ... 22.1)	<n.e>

MPI-ESM1-2-LR_historical-ssp585	reasonable	reasonable	18.1 (13.8 ... 21.3)	101.77
MRI-ESM2-0_historical-ssp585	bad	reasonable	17.2 (13.9 ... 19.7)	<n.e>
NESM3_historical-ssp585	bad	reasonable	17.3 (12.9 ... 20.1)	<n.e>
NorESM2-LM_historical-ssp585	good	reasonable	20.4 (15.9 ... 23.6)	<n.e>
NorESM2-MM_historical-ssp585	reasonable	reasonable	21.0 (14.5 ... 26.1)	<n.e>
UKESM1-0-LL_historical-ssp585	bad	bad	64.5 (52.6 ... 73.9)	<n.e>
EC-EARTH3P	bad	good	11.0 (8.26 ... 13.1)	63.89
EC-EARTH3P-HR	reasonable	reasonable	9.89 (7.30 ... 11.9)	69.283
HADGEM3-GC31-LM	reasonable	good	20.5 (14.7 ... 24.7)	87.699
HADGEM3-GC31-MM	reasonable	good	18.6 (15.6 ... 20.5)	93.575
HADGEM3-GC31-HM	reasonable	good	19.4 (15.5 ... 22.2)	92.405
CMCC-CM2-HR4	reasonable	good	19.5 (13.8 ... 23.8)	96.371
CMCC-CM2-VHR4	reasonable	good	16.0 (11.6 ... 19.8)	100.24
CNRM-CM6-1	reasonable	good	19.0 (14.3 ... 22.4)	61.504
MPI-ESM1-2-HR	bad	good	8.90 (6.77 ... 10.3)	73.122
MPI-ESM1-2-XR	bad	good	8.12 (7.03 ... 9.02)	74.261
AM2.5C360	good	good	17.8 (15.7 ... 19.6)	102.25
FLOR	bad	reasonable	27.8 (26.2 ... 29.2)	81.101
CanESM2-CanRCM4	bad	bad	15.2 (10.8 ... 18.5)	139.89
CNRM-CM5_r1i1p1_CCLM4-8-17	reasonable	reasonable	22.9 (18.1 ... 26.1)	98.946
EC-EARTH_r12i1p1_CCLM4-8-17	bad	good	21.1 (16.9 ... 24.4)	89.553
EC-EARTH_r12i1p1_RACMO22T	bad	reasonable	14.1 (7.55 ... 19.6)	58.959
EC-EARTH_r12i1p1_REMO2009	bad	good	21.1 (16.6 ... 24.5)	81.922
EC-EARTH_r1i1p1_RACMO22T	bad	reasonable	16.8 (13.1 ... 19.5)	62.805
EC-EARTH_r3i1p1_HIRHAM5	reasonable	good	12.8 (9.55 ... 15.6)	78.17
IPSL-CM5A-LR_r1i1p1_REMO2009	good	good	15.1 (11.9 ... 17.6)	77.284
MIROC5_r1i1p1_REMO2009	good	good	13.1 (9.63 ... 15.7)	88.589
HadGEM2-ES_r1i1p1_CCLM4-8-17	bad	good	21.7 (16.7 ... 25.0)	83.692
HadGEM2-ES_r1i1p1_REMO2009	good	good	16.6 (13.3 ... 19.0)	87.436
HadGEM2-ES_r1i1p1_RegCM4-3	bad	good	18.3 (13.7 ... 21.6)	81.134
HadGEM2-ES_r1i1p1_RACMO22T	bad	reasonable	22.6 (17.8 ... 25.7)	72.509
MPI-ESM-LR_r1i1p1_CCLM4-8-17	reasonable	good	21.6 (15.8 ... 25.2)	74.138
MPI-ESM-LR_r1i1p1_REMO2009	good	good	17.4 (11.9 ... 21.7)	81.397

MPI-ESM-MR_r1i1p1_RegCM4-3	bad	good	23.7 (18.0 ... 27.8)	69.233
GFDL-ESM2G_r1i1p1_REMO2009	good	good	17.8 (11.7 ... 22.2)	84.028
HadGEM2-ES_r1i1p1_CCLM5-0-15	reasonable	bad	20.9 (15.5 ... 25.1)	96.644
HadGEM2-ES_r1i1p1_REMO2015	good	good	14.5 (10.1 ... 17.6)	89.585
HadGEM2-ES_r1i1p1_RegCM4-7	reasonable	good	19.2 (14.4 ... 22.9)	67.506
MPI-ESM-LR_r1i1p1_CCLM5-0-15	good	good	21.5 (17.2 ... 24.7)	74.746
MPI-ESM-LR_r1i1p1_REMO2015	good	good	15.3 (10.8 ... 18.4)	81.482
MPI-ESM-MR_r1i1p1_RegCM4-7	bad	good	13.6 (10.9 ... 15.4)	52.645
NorESM1-M_r1i1p1_CCLM5-0-15	bad	good	16.6 (11.9 ... 20.0)	78.529
NorESM1-M_r1i1p1_REMO2015	reasonable	good	22.9 (18.3 ... 26.2)	83.231
NorESM1-M_r1i1p1_RegCM4-7	bad	good	11.7 (9.36 ... 13.3)	46.46

Central Sahel and more broadly West Africa are located within the gradient of monsoon rainfall climatology, which makes results sensitive to the representation of the monsoon location in models. As a result, many models fail to capture one of the features used for model evaluation. For CMIP6 overall, 5 models out of the 19 evaluated are selected for the total June precipitation indicator (Table 1), 4/19 models for the rainy season onset indicator (Table 2), and 4/19 models for the rainy season duration (Table 3). As CMIP6 data are here bias-corrected, most of the models do capture a satisfying spatial pattern of rainfall over West Africa. However, it also results in “bad” seasonal cycles for many models, which downsizes the final CMIP6 models number kept for the attribution analysis.

From the CORDEX ensemble at 0.44º resolution, 1/17 models was retained for the total June precipitation (Table 1), with the remainder rejected due to lack of agreement with the parameters of the observed distribution of June precipitation, generally due to overdispersion in the models; 5/17 for the rainy season onset (Table 2); and 6/17 were retained for the rainy season duration (Table 3). At 0.22º resolution, no models were retained for the total June precipitation (Table 1), again due to overdispersion in the distribution of June precipitation in the models; 3/9 were retained for the rainy season onset (Table 2); and 4/9 were retained for the rainy season duration (Table 3). Of the ten HighResMIP models evaluated, four were retained for total June precipitation (Table 1); two for the rainy season onset (Table 2); and four were retained for the rainy season duration (Table 3). The HighResMIP models are forced with observed SSTs, and only used in the attribution of changes prior to the present climate.

The FLOR ensemble is not retained for the synthesis since it is not able to capture the observed seasonal cycle, perhaps due to its relatively coarse horizontal resolution (~50 km) compared to the area of the analysed region or the simulated SST bias from the coupled model. The AM2.5C360 ensemble, which has a higher resolution of about 25 km, reproduces the seasonal cycle well and has a reasonable dispersion parameter for the June rainfall. However, the sigma parameters for the rainy season onset and duration are too large and out of the observational confidence interval. Therefore, the AM2.5C360 ensemble result is only retained for the June rainfall synthesis but not for the rainy season onset and duration.

The performance of all the models over Central Sahel and for all of the three indicators chosen to conduct this attribution study is recorded in Table 1-3.

5 Multi-model attribution

This section shows Probability Ratios and change in intensity ΔI for models and also includes the values calculated from the fits with observations. Results are shown for each of the event definitions in turn for the current climate relative to a 1.2℃ cooler climate (before anthropogenic climate change) as well as a future 2.0℃ warmer climate with results relative to the current climate.

***Table 4**: Probability ratio and change in intensity of June precipitation in the current climate when compared with (a) a 1.2°C cooler climate and (b) a 2°C warmer climate from the models that passed the validation tests.*

Model / Observations	(a) Past vs. present		(b) Present vs. future	
	Probability ratio PR [-]	Change in intensity ΔI [%]	Probability ratio PR [-]	Change in intensity ΔI [%]
CHIRPS	0.078 (0.015 ... 0.29)	1.2e+2 (43 ... 2.3e+2)		
TAMSAT	0.11 (0.031 ... 0.26)	1.9e+2 (83 ... 3.3e+2)		
MSWEP	0.75 (0.19 ... 3.3)	20 (-52 ... 2.2e+2)		
ACCESS-CM2 historical-ssp585	0.83 (0.47 ... 1.8)	14 (-23 ... 1.1e+2)	1.0 (0.93 ... 1.1)	-0.057 (-5.5 ... 5.0)
BCC-CSM2-MR historical-ssp585	0.20 (0.085 ... 0.48)	55 (19 ... 1.1e+2)	1.6 (1.3 ... 2.4)	-17 (-23 ... -9.7)
CNRM-CM6-1-HR historical-ssp585	1.3 (0.69 ... 2.0)	-15 (-40 ... 22)	1.0 (0.90 ... 1.1)	-0.72 (-5.1 ... 4.9)
IPSL-CM6A-LR historical-ssp585	0.81 (0.40 ... 1.8)	17 (-31 ... 1.1e+2)	0.94 (0.84 ... 1.1)	4.1 (-2.4 ... 13)
MPI-ESM1-2-LR historical-ssp585	1.4 (0.24 ... 3.6)	-18 (-54 ... 59)	0.97 (0.73 ... 1.3)	0.92 (-6.0 ... 9.4)
HADGEM3-GC31-MM highresSST	1.8 (0.97 ... 4.6)	33 (-1.3 ... 84)	<n.e>	<n.e>
HADGEM3-GC31-HM highresSST	0.62 (0.31 ... 1.2)	22 (-6.3 ... 57)	<n.e>	<n.e>
CMCC-CM2-HR4 highresSST	0.73 (0.26 ... 1.8)	12 (-18 ... 50)	<n.e>	<n.e>
CMCC-CM2-VHR4 highresSST	0.40 (0.19 ... 0.69)	37 (13 ... 75)	<n.e>	<n.e>
CNRM-CM5_r1i1p1_CCLM4-8-17	1.5 (0.71 ... 3.6)	-11 (-28 ... 11)	0.93 (0.65 ... 1.2)	2.6 (-6.5 ... 13)
AM2.5C360	1.5 (1.1 … 2.3)	-13 (-23 ... -2.6)	1.5 (1.3 ... 1.8)	-14 (-20 ... -8.8)

***Table 5**: Probability ratio and change in intensity of rainy season onset in the current climate when compared with (a) a 1.2°C cooler climate and (b) a 2°C warmer climate from the models that passed the validation tests.*

Model / Observations	(a) Past vs. present		(b)Present vs. future	
	Probability ratio PR [-]	Change in intensity ΔI [day of the year]	Probability ratio PR [-]	Change in intensity ΔI [day of the year]
CHIRPS	3.4 (0.30 ... 95)	8.2 (-8.5 ... 25)		
TAMSAT	1.2 (0.14 ... 18)	1.3 (-15 ... 19)		
MSWEP	3.2 (0.6 ... 39)	13.1 (-6.6 ... 34)		
CMCC-CM2-HR4 highresSST	1.3 (0.50 ... 3.9)	4.4 (-9.7 ... 19)	<n.e>	<n.e>
CMCC-CM2-VHR4 highresSST	1.1 (0.46 ... 2.6)	1.4 (-9.7 ... 12)	<n.e>	<n.e>
ACCESS-CM2 historical-ssp585	8.6 (2.1 ... 53)	20 (6.5 ... 33)	<n.e>	<n.e>

BCC-CSM2-MR historical-ssp585	0.38 (0.16 ... 0.72)	-18 (-27 ... -7.0)	<n.e>	<n.e>
CNRM-CM6-1-HR historical-ssp585	2.0 (0.66 ... 6.8)	8.5 (-4.8 ... 22)	<n.e>	<n.e>
IPSL-CM6A-LR historical-ssp585	0.77 (0.33 ... 1.7)	-3.8 (-15 ... 8.2)	<n.e>	<n.e>
MIROC6 historical-ssp585	1.9 (0.69 ... 7.5)	8.5 (-5.1 ... 24)	<n.e>	<n.e>
MPI-ESM1-2-LR historical-ssp585	3.5 (0.85 ... 14)	13 (-1.8 ... 29)	<n.e>	<n.e>
EC-EARTH_r3i1p1_HIRHAM5	0.94 (0.36 ... 1.9)	-0.60 (-8.8 ... 7.1)	0.78 (0.64 ... 1.0)	-3.0 (-6.2 ... 0.12)
IPSL-CM5A-LR_r1i1p1_REMO2009	1.6 (0.74 ... 3.8)	4.6 (-3.1 ... 13)	0.85 (0.69 ... 1.1)	-1.9 (-5.1 ... 1.1)
MIROC5_r1i1p1_REMO2009	3.1 (1.3 ... 8.8)	9.7 (2.3 ... 18)	0.71 (0.61 ... 0.90)	-4.5 (-7.5 ... -1.2)
HadGEM2-ES_r1i1p1_REMO2009	1.2 (0.62 ... 2.1)	2.0 (-4.6 ... 8.7)	1.1 (0.90 ... 1.3)	0.83 (-1.3 ... 2.8)
MPI-ESM-LR_r1i1p1_REMO2009	0.94 (0.36 ... 2.0)	-0.92 (-12 ... 9.6)	1.2 (0.95 ... 1.8)	2.5 (-0.63 ... 5.6)
HadGEM2-ES_r1i1p1_REMO2015	0.87 (0.38 ... 1.6)	-1.2 (-6.6 ... 4.3)	1.3 (1.0 ... 1.9)	1.9 (-0.031 ... 3.9)
HadGEM2-ES_r1i1p1_RegCM4-7	0.62 (0.26 ... 1.1)	-10 (-26 ... 2.3)	1.2 (0.93 ... 1.5)	2.2 (-1.0 ... 5.5)
MPI-ESM-LR_r1i1p1_REMO2015	0.54 (0.20 ... 1.2)	-11 (-24 ... 3.7)	1.6 (1.1 ... 2.8)	5.6 (1.5 ... 9.6)

***Table 6**: Probability ratio and change in intensity of rainy season duration in the current climate when compared with (a) a 1.2°C cooler climate and (b) a 2°C warmer climate from the models that passed the validation tests.*

Model / Observations	(a) Past vs. present		(b) Present vs. future	
	Probability ratio PR [-]	**Change in intensity ΔI [days]**	**Probability ratio PR [-]**	**Change in intensity ΔI [days]**
CHIRPS	1.2 (0.15 ... 22)	-1.5 (-22 ... 18)		
TAMSAT	0.61 (0.16 ... 3.7)	6.7 (-14 ... 27)		
MSWEP	4.2 (0.7 ... 51)	-17 (-38.6 ... 4.3)		
EC-EARTH3P-HR highresSST	0.48 (0.22 ... 0.96)	9.1 (0.55 ... 16)	<n.e>	<n.e>
CMCC-CM2-HR4 highresSST	0.98 (0.42 ... 2.3)	0.40 (-14 ... 15)	<n.e>	<n.e>
CMCC-CM2-VHR4 highresSST	0.67 (0.26 ... 1.5)	7.4 (-6.9 ... 23)	<n.e>	<n.e>
CNRM-CM6-1 highresSST	0.60 (0.30 ... 1.2)	12 (-5.2 ... 28)	<n.e>	<n.e>
ACCESS-CM2 historical-ssp585	1.8 (0.46 ... 5.6)	-7.0 (-21 ... 7.3)	0.40 (0.018 ... 1.1)	22 (-5.4 ... 75)
BCC-CSM2-MR historical-ssp585	1.3 (0.47 ... 3.5)	-3.1 (-16 ... 9.3)	0.35 (0.031 ... 1.1)	33 (-1.4 ... 67)
IPSL-CM6A-LR historical-ssp585	0.73 (0.30 ... 1.7)	4.6 (-7.4 ... 17)	0.94 (0.83 ... 1.1)	0.76 (-0.72 ... 2.1)
MPI-ESM1-2-LR historical-ssp585	1.6 (0.58 ... 4.5)	-6.9 (-19 ... 8.1)	0.81 (0.66 ... 0.96)	4.0 (0.84 ... 7.0)
CNRM-CM5_r1i1p1_CCLM4-8-17	1.7 (0.48 ... 6.0)	-9.9 (-30 ... 12)	0.72 (0.58 ... 0.90)	7.7 (1.9 ... 13)
EC-EARTH_r3i1p1_HIRHAM5	1.5 (0.58 ... 3.4)	-4.2 (-14 ... 4.8)	0.71 (0.60 ... 0.87)	4.8 (1.6 ... 7.9)
IPSL-CM5A-LR_r1i1p1_REMO2009	1.1 (0.54 ... 1.9)	-0.85 (-10 ... 8.0)	1.0 (0.82 ... 1.3)	-0.020 (-2.9 ... 3.0)
MIROC5_r1i1p1_ REMO2009	1.5 (0.59 ... 4.0)	-4.8 (-15 ... 5.5)	0.81 (0.67 ... 1.1)	3.2 (-0.87 ... 7.4)
HadGEM2-ES_r1i1p1_REMO2009	0.79 (0.36 ... 1.3)	3.9 (-4.6 ... 14)	1.2 (0.97 ... 1.7)	-2.7 (-6.0 ... 0.50)
MPI-M-MPI-ESM-LR_r1i1p1_REMO2009	1.2 (0.51 ... 2.5)	-3.0 (-15 ... 9.3)	1.0 (0.82 ... 1.4)	-0.61 (-4.5 ... 3.6)
HadGEM2-ES_r1i1p1_REMO2015	0.77 (0.25 ... 1.5)	3.8 (-6.1 ... 15)	1.2 (0.92 ... 1.7)	-1.9 (-5.2 ... 1.1)
HadGEM2-ES_RegCM4	0.59 (0.20 ... 1.0)	11 (-0.098 ... 23)	1.1 (0.90 ... 1.4)	-1.2 (-4.2 ... 1.8)
MPI-ESM-LR_r1i1p1_CCLM5-0-15	1.3 (0.52 ... 2.7)	-4.3 (-18 ... 9.1)	1.0 (0.84 ... 1.4)	-0.58 (-4.7 ... 3.7)
MPI-ESM-LR_r1i1p1_REMO2015	0.93 (0.30 ... 3.0)	1.1 (-17 ... 16)	1.4 (0.98 ... 2.3)	-4.5 (-9.4 ... 0.30)

6 Hazard synthesis

For the event definitions described above we evaluate the influence of anthropogenic climate change on the event by calculating the probability ratio and the change in intensity using observations (in this case: CHIRPS, TAMSAT and MSWEP datasets) and models. Models which do not pass the validation tests described above are excluded from the analysis. The aim is to synthesise results from models that pass the evaluation along with the observations, to provide an overarching attribution statement. To combine observations and models into a synthesised assessment (see Figures 6-9), first, a representation error is added (in quadrature) to the observations, to account for the difference between observations-based datasets that cannot be explained by natural variability. This is shown in these figures as white boxes around the light blue bars. The dark blue bar shows the average over the observation-based products. Next, a term to account for intermodel spread is added (in quadrature) to the natural variability of the models if necessary. This is shown in the figures as white boxes around the light red bars. The dark red bar shows the model average, consisting of a weighted mean using the (uncorrelated) uncertainties due to natural variability plus the term representing intermodel spread (i.e., the inverse square of the white bars). Observations and models are combined into a single result, in two ways if they seem to be compatible. Firstly, we neglect common model uncertainties beyond the model spread that is depicted by the model average, and compute the weighted average of models and observations: this is indicated by the magenta bar in Figures 6-8. As due to usual model uncertainties, model uncertainty can be larger than the model spread, secondly we show the more conservative estimate of an unweighted average of observations and models, indicated by the white box around the magenta bar in the synthesis figures. For both event definitions only few models pass the evaluation. The remaining models as well as the three observational datasets show very different results and large uncertainties. Due to these large uncertainties, we refrain from quantifying the role of anthropogenic climate change. As a conclusion, for the indices and data used, it is impossible to find a significant change in the monsoon season characteristics that is linked with climate change up to now.

Projecting the changes in likelihood and intensity for a 0.8℃ warmer future for the models that easily had the future climate available, Figures 9-11, also show large discrepancies between the models. As for the current climate, the models show no trend emerging clearly from natural variability.

We stress here that despite our analysis does not show significant trends for three specific indices characterising the anomaly of the 2021 rainy season, other indices may be defined, but have not been studied here. Therefore we refrain from concluding about the absence of a climate change effect in this case.

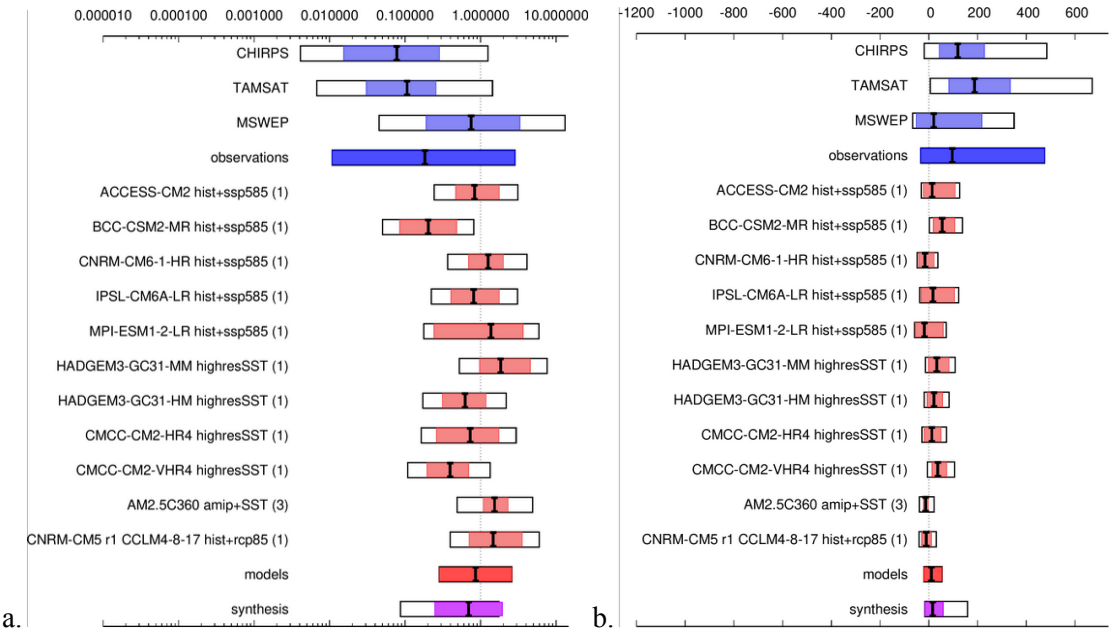

Figure 6: Synthesis of (a) probability ratios and (b) intensity changes when comparing the return period and magnitudes of the total precipitation in June 2021, in the current climate and a 1.2°C cooler climate.

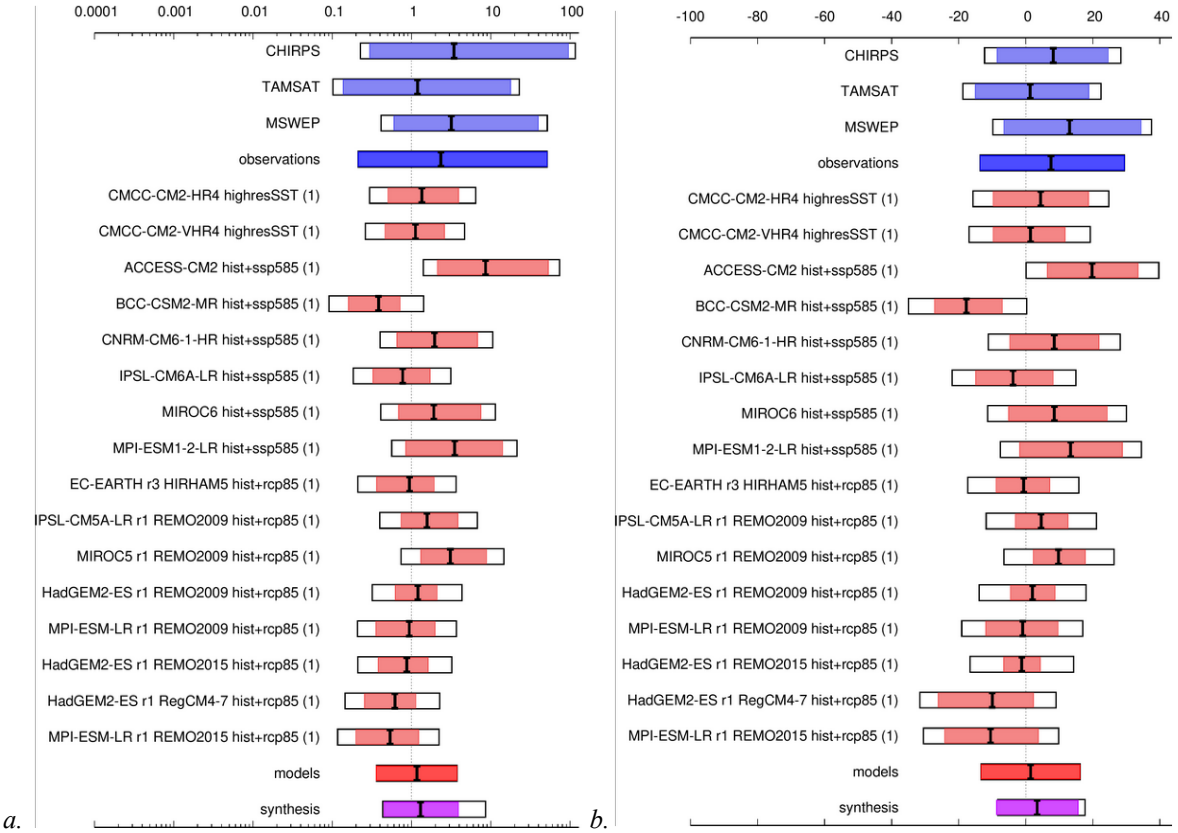

Figure 7: Synthesis of (a) probability ratios and (b) intensity changes when comparing the return period and magnitudes of the onset of the 2021 rainy season, in the current climate and a 1.2ºC cooler climate.

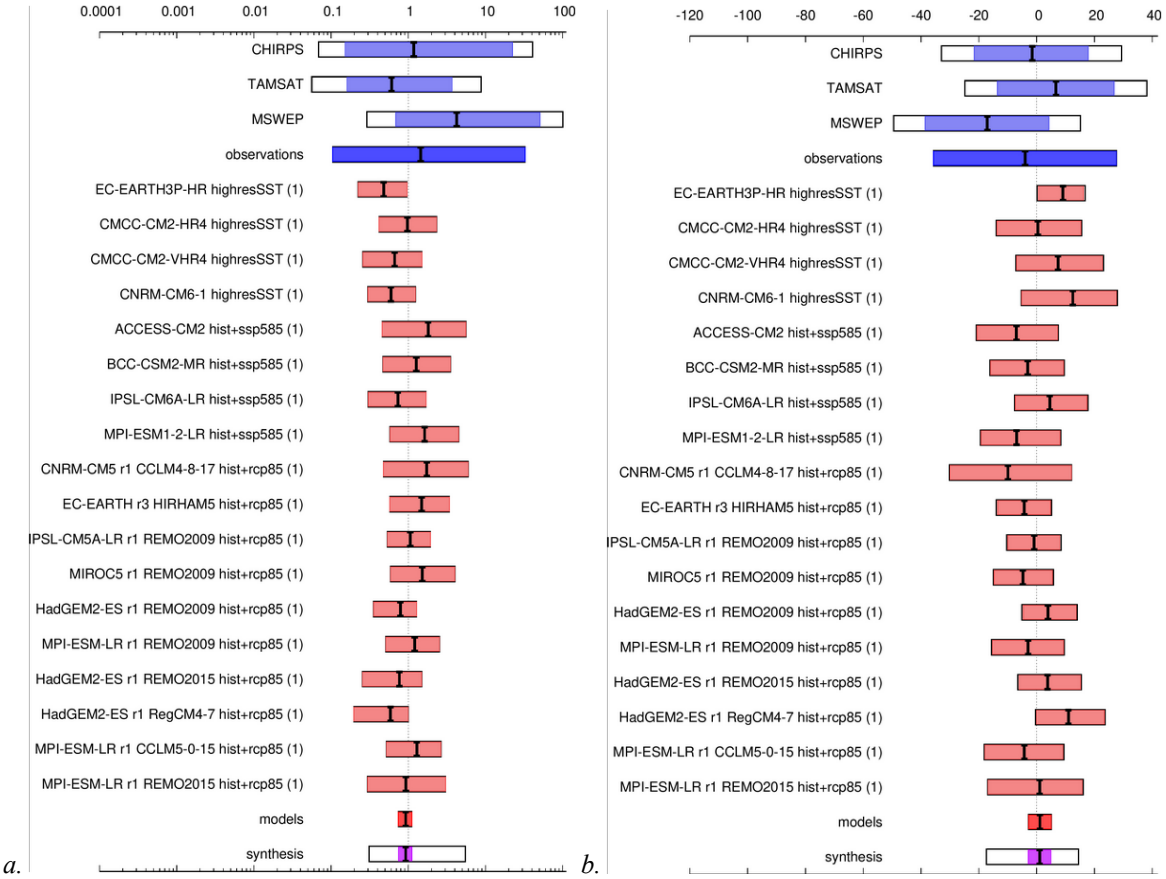

Figure 8: Synthesis of (a) probability ratios and (b) intensity changes when comparing the return period and magnitudes of the duration of the 2021 rainy season, in the current climate and a 1.2ºC cooler climate.

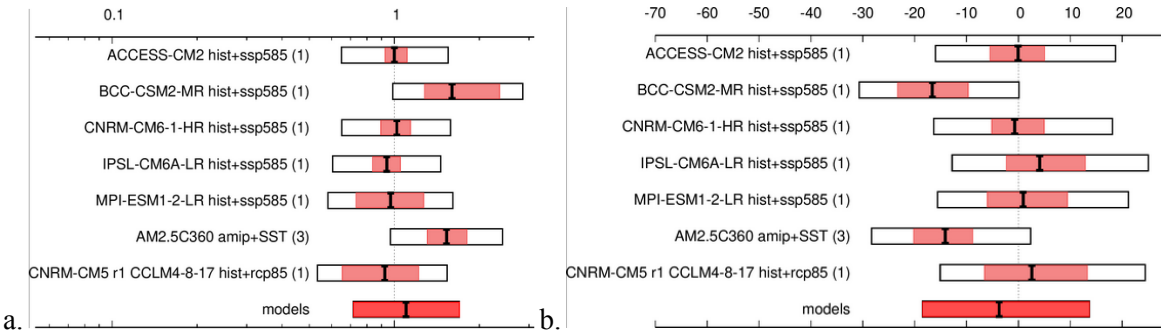

Figure 9: As in Figure 6, but for models only of a 0.8ºC warmer (2ºC since pre-industrial) climate.

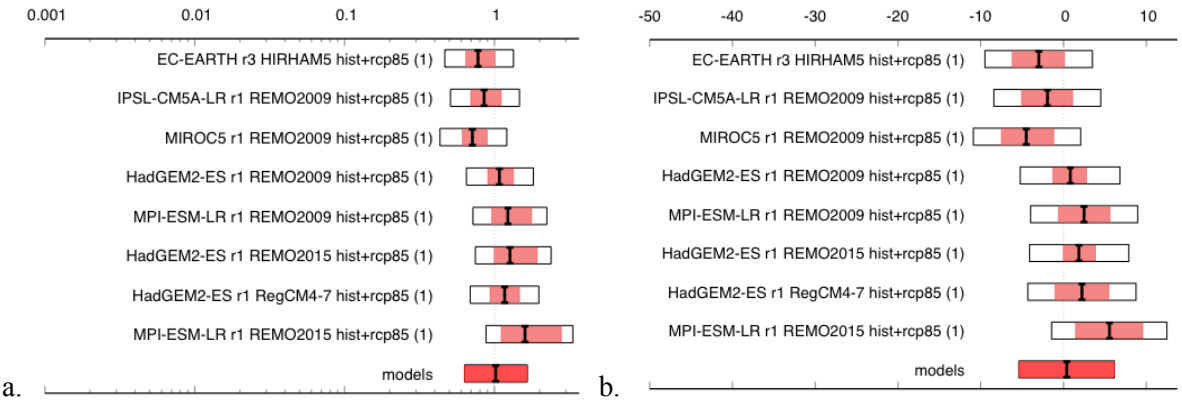

Figure 10: As in Figure 7, but for models only of a 0.8ºC warmer (2ºC since pre-industrial) climate.

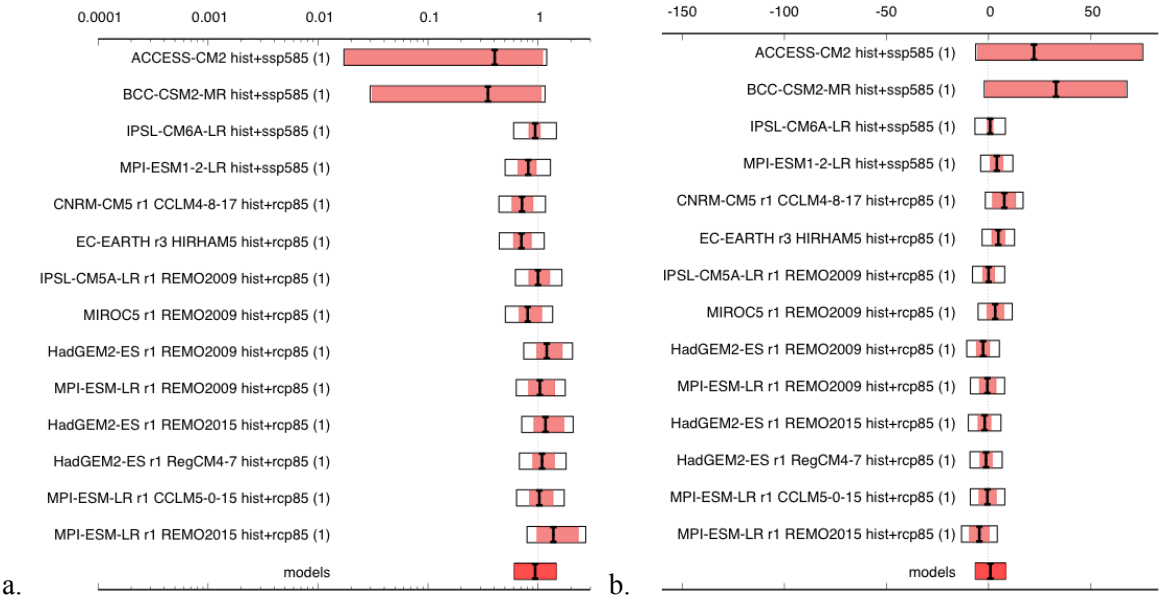

Figure 11: As in Figure 8, but for models only of a 0.8ºC warmer (2ºC since pre-industrial) climate.

7 Vulnerability and exposure

Risk is a combination of a hazard, and the exposure, vulnerability, and coping capacity of people, infrastructure, and human systems in the face of the shock (IPCC SREX, 2012; Raju, Boyd and Otto, 2022). The impacts of the West African drought must be understood as a product of these factors, and thus the following section outlines the key vulnerability and exposure themes which are contributing to the impacts described in previous sections. We find that these impacts are a combination of the livelihood profile of the region, chronic and differential vulnerability, compound impacts of past extreme weather and global forces, a difficult political situation with migration and conflict driving elevated vulnerability. Various coping strategies, adaptation, humanitarian, and social protection measures can help increase resilience and minimise impacts from these types of events in the future.

7.1 Climate, livelihoods and chronic vulnerability

The climate of the Sahel exhibits large shifts in rainfall over periods of multiple decades. For example, historical data shows a significant wet period in the 1950s and 60s, followed by a prolonged period of drought from the 1970s to the 1990s, and a recovery in rainfall amounts since the early 2000s (Becker et al., 2013). In recent years, there is an emerging trend for wetter rather than drier years, especially starting in the 2000s (Haarsma et al., 2005; Bichet and Diedhiou, 2018). While average rainfall over the rainy season is normal or above-normal in recent years, the character of that rainfall may have changed with more dry days interspersed with intense rainfall events (Giannini et al., 2013, Haarsma et al., 2005, Lodoun et al., 2013). Mean teamperatures across the Sahel have increased since the 1970's and heatwaves have also become hotter and longer; these trends are projected to continue with the number of hot days and heatwaves expected to rise under all emissions scenarios (IPCC WG2 CH9). According to a systematic review of studies looking at the impacts of climate change on crop yields in West Africa, a robust consensus is emerging of agricultural yeild losses linked to climate change (Sultan and Gaetani, 2016). Interestingly, the review indicates that this is primilarly due to higher temperatures leading to higher evapotranspirtion and a shortening the crop cycle duration, and occur regardless of changes to rainfall (Sultan and Gaetani, 2016). An increase in rainfall can moderate this effect, while a reduction can increase yield losses (Sultan and Gaetani, 2016).

Poor timing and spatial distribution of rains is often cited in EVIAM (Enquête Conjointe sur la Vulnérabilité à l'Insécurité Alimentaire des Ménages) food security assessments reports as a factor contributing to poor harvest and food insecurity (STAT Niger). This includes late onset of rains, premature stop, dry spells, and localized rainfall conditions differing from village to village. Further, for farmers it is not just lack of rainfall that is a concern, but too much rainfall can lead to flooding and waterlogged fields, and damage to food stocks which can also negatively impact food security, as was the case in August and September 2022 when locally torrential rains in Burkina Faso and Niger damaged infrastructure and stocks (FEWSNET, 2022; ECHO Daily Flash, 2022).

The Sahel is a chronically food insecure region with infrastructure in place to assess and anticipate food needs each year (Mbow et al., 2021). National governments, the Economic Community of West African States (ECOWAS), the West African Economic and Monetary Union (UEMOA), United Nations agencies, non-governmental organisations, and international organisations conduct an annual assessment of food security using the Cadre Harmonisé (IPC). This is a region-wide food security and nutrition assessment and projection tool and is intended to support decision-making on emergency response.

Countries such as Mali, Niger, Chad, and Burkina Faso rank towards the bottom of the 2021 Human Development Index: 186, 189, 190, and 184, respectively, out of 191 (UNDP, 2022). Pastoralism and rain-fed agriculture are the main types of livelihoods in the Sahel, and are highly reliant on a single rainy season from June-September (World Bank, 2021; Feed the Future, n.d.; IFAD, 2020; Ado et al., 2019). The agricultural sector employs 73 and 75 percent of the working populations (World Bank, 2019a; World Bank, 2019b), and accounts for about 36.37 and 53.99 percent of GDP for Niger and Chad, respectively (Statista, 2021a; Statista, 2021b). The INFORM Subnational Risk indices for Chad and Niger show that risk is highest in the countries' agricultural heartland around Lake Chad (DRMKC, 2019a; DRMKC, 2019b; Okpara, Stringer and Dougill, 2016), giving further testament to pastoralists' and farmers' precarious living conditions. Further, gender disparities are wide in education, livelihoods, incomes, access to property and these factors contribute to exacerbating

women's vulnerabilities. Climate change related impacts are also reflected in the amount of time women need to spend on gathering water, and other livelihood needs while continuing with household chores (Tarif, 2022; McOmber, 2020). As extreme heat increases in the Sahel, impacts such as reduced labour productivity are already evident with the International Labour Office reporting that seven of the 10 countries most severely affected by labour productivity loss due to heat stress are in the Sahel, with agricultural workers amongst the most impacted (ILO, 2019). Countries in the Sahel face extreme poverty, social and political tensions, institutional and governance challenges, weak or lacking infrastructure (e.g. healthcare facilities, roads, sanitation facilities, electricity), violent extremism and militancy, and environmental degradation which contribute in direct and indirect ways to the food insecurity crisis (Al Saidi et al., 2022, Hummel et al., 2015; UNDP, 2019).

7.2 Conflict and political unrest

Armed conflict is a key driver of instability and increasing vulnerability for populations in the Sahel. In Burkina Faso, Mali, Chad and Niger, an insurgency of armed groups since 2011 has forced many people to flee their homes with over three million people internally displaced, and over one million becoming refugees in neighbouring countries (UNHCR, 2022). In Burkina Faso, a military coup in January 2022 was followed by a second coup on September 30th, increasing political instability in the country, and was, at least in part, driven by an inability of the government to deal with a worsening armed uprising in parts of the country (Aljazeera, 2022).

A widespread increase in violent incidents has caused large-scale displacement in 2022, forcing many rural households to abandon their crops and move (FAO, 2022). During the first half of 2022, the increase in attacks by armed groups in Mali, Burkina Faso and northern Nigeria led to 36,000 people crossing the border into Niger, the majority of whom are women and children (Save the Children, 2022). According to the government, 61.7% of the internally displaced persons (IDPs) are from Burkina Faso, which equals 1.9 million people who were internally displaced at the end of April 2022 (UNHCR, 2022). With progressing impacts from climate change, it is expected that displacement will increase in already-vulnerable countries (IPCC WGII, chapter 16, IDMC, 2022b). Conflict often results in a reduction in the number of cultivated hectares of cropland, due to a multitude of reasons including mass displacement and militant takeovers of areas (Cold-Ravnkilde, 2022). In Mali, elected representatives and local officials have fled violent conflict, leading to areas without any government support where people fear leaving their homes in urban areas, are unable to travel freely to reach their fields, move their herds or go to neighbouring areas to conduct commerce (ICRC, 2020). The conflict has disrupted the development of basic infrastructure and services such as healthcare, and reversed development gains (ICRC, 2020).

A systematic literature review reveals that climate change and violent conflict intersect when (a) maladaptation accentuates local resource competition; (b) increasing migration, as an adaptation strategy, increases resource competition in areas less impacted by climate change; (c) weak governance provides armed groups with new opportunities or leads to increased reliance on armed self-defence; and (d) weak and sometimes divisive governance increases climate vulnerability, feeds local grievances and drives violent conflicts (Tarif, 2022). However, the IPCC indicates a decrease in precipitation in the western Sahel, while in the central Sahel, the study region, there may be an increase overall (IPCC). Governance is critical when it comes to the conflict risks associated with

climate change in the region and addressing insecurity in climate-exposed regions requires the prioritisation of legitimate and inclusive governance mechanisms is prioritised (Tarif, 2022).

7.3 Migration as a coping strategy

Transhumance, the seasonal movement of livestock for feed and water, has been the way of life and a coping strategy for climate variability in the Sahel for hundreds of years (UN, 2020, Stavi et al., 2021). However, the competition for land, water and forage has led to conflicts, primarily between sedentary farmers and transhumant pastoralists, but also fishermen and illegal miners (UNOWAS, 2019). Farmers and pastoralists report that changing climatic conditions have made the competition for resources intense, as longer dry spells and short bursts of rainfall are more common rather than steady rainfall throughout the rainy season (UNOWAS, 2019; ICRC, 2020). Further, increased direct heat stress, and reduced availability of forage linked to higher rainfall variability, can also negatively impact livestock (IPCC).

In 2020, many pastoralists were affected by COVID-19 related border closures, especially along the Central Transhumance Corridor (CTC) that links the Sahel to markets and resources in the south leaving herders stranded and unable to access fodder or water, and forcing some to reduce their herd sizes (Griffith et al., 2021). Similar to the food insecurity drivers in Madagascar (Harrington et al., 2021), road and market closures due to the pandemic also resulted in reduced income for pastoralists, and restricted access to food, especially impacting women whose role is often to purchase vegetables and grain from markets (Griffith et al., 2021).

Conflict, unreliable rainfall, and economic conditions are driving people to move to cities in search of work, or to seasonally migrate to artisanal gold mining sites or to countries such as the Cote d'Ivoire in search of seasonal work during the dry season (ICRC, 2020).

7.4 Global influences

Across Sahelian countries, cereal and grain prices have recently spiked by exceptional proportions. Despite the 2022 forecast asserting a cereal output higher than the five-year average, food prices are soaring. By August 2022, prices of maize, millet, and sorghum - key ingredients in West African staple foods - had risen by up to 60 percent in Chad, while Niger saw food price increases of 40 percent (FAO, 2022). The low yields in 2021, limitations to the export of cereal-based products, as well as regional economic sanctions have all played a role in decreasing the cereal availability in the countries (FAO, 2022). Notably, there are three global influences which further exacerbate the crisis; an international decline in wheat availability, the COVID-19 pandemic, and insufficient funding of Niger and Chad's respective humanitarian response plans (ALIMA, 2022; OXFAM, 2022).

While wheat is not a staple crop in the Sahel, West Africa imports of wheat from both Russia and Ukraine, and the decrease in wheat output and disruption of trade flows caused by the Ukraine war may have further aggravated the region's food insecurity (Petesch, 2022; IMF Blog, 2022). Food security for pastoralists across Sahel has also been markedly impacted by the COVID-19 pandemic, due to reduced access to key inputs for livestock production, including animal health services (e.g. livestock vaccination), livestock feeds, and access to pasture and water (Griffith et al., 2021; ECOWAS, 2022). In Burkina Faso the COVID-19 pandemic resulted in reduced incomes and

remittances for poor households, which combined with higher food prices led to higher food insecurity (Zidouemba, Kinda and Ouedraogo., 2020). Despite social protection programmes such as *Wadata Talaka*, which was scaled up from supporting 28.000 to 400.000 households with cash payments during the pandemic (Brunelin et al., 2022), extreme poverty over West Africa rose by approximately three percent throughout 2021 (ECOWAS, 2022) - further reducing people's abilities to meet their basic needs.

Niger and Chad's humanitarian response plans remain underfunded, with less than half of the countries' appeals funded (FTS, 2022a; FTS, 2022b). While Chad's response plan has been allocated more funding in 2022 compared to 2021, the appeal is still only funded by just over one-third (FTS, 2021a; FTS, 2022b). Niger, on the other hand, has lost its funding by ten percentage points over the same period of time (FTS, 2021b; FTS, 2022a). That a crisis of this magnitude remains underfunded poses lethal risks to the tens of millions of people who are suffering from hunger.

7.5 Adaptation

The complexities of drought and compound events are such that a wide range of strategies are taken to decrease the impact of these hydrometeorological phenomena (Raymond et al., 2020). These include regional, national, and local water and agricultural management policies and structures, climate change adaptation plans and commitments, and community and household-level humanitarian action. At seasonal and subseasonal scales, Early Warning Early Action (EWEA) tools such as crop monitoring, food insecurity tracking, and early warning communication can prove essential decision-making support.

Several large development projects are also operational in the region aiming at supporting livelihoods, gender equity, economic development, health, and more. For instance, UNDP and the Swedish government are currently running a 7.5 million USD project called the *Sahel Resilience Project (*UNDP, n.d.*);* the *Regional Joint Programme Sahel in Response to the Challenges of COVID-19 programme* was launched in 2021 by the International Fund for Agricultural Development with a budget of 180.4 million USD (IFAD, 2021); a range of partners including the United Nations Office of the Special Coordinator for Development in the Sahel have also committed 1.6 billion USD over five years to support the resilience and development of the Sahel (Generation Unlimited, 2021); in September 2020, the African Development Bank was running 105 projects in the different countries of the region with total commitments of 3.2 billion (AfDB, 2022).

Food security projects are particularly common, with projects such as the Nigeriens Nourish Nigeriens and the Food Security Support Project in the Maradi region have contributed to Niger's adaptation goals and strides, with the former having played a key role in halving the country's proportion of people suffering from hunger since 2011 (Future Policy, n.d). Across Sahel, income diversification and water management, notably water harnessing, have been found to be the most implemented adaptation actions (Epule, Chehbouni and Dhiba, 2021).

Irrigation in the Sahel, while not current commonly used, has large potential with abundant surface water and groundwater for transforming and diversifying agricultural productivity, on the one hand, and improving the livelihoods of rural communities, on the other (UNCCD, 2019). The region is exploring a large-scale irrigation approach and the CILSS is engaged in projects like the Sahel

Irrigation Initiative Support Project (PARIIS-SIIP). Despite the significant potential of sustainable irrigation, van der Wijngaart et al. (2019) find that the cost of realising it is higher than most other places across the world, which is central to why rain-fed agricultural practices are still considered most viable and cost-effective.

Farmers' strategies for dealing with food deficits take different forms. The main strategy is rural-urban migration. People between the ages of 18 and 40 leave their villages at the end of the rainy season to look for work in big cities or abroad. This exodus not only reduces the number of mouths to feed per family but also, for some, postpones the consumption of agricultural production. The contents of the granaries are thus reserved for the lean season, when weeding takes place. Another strategy is the sale of crop residues.With regard to pastoralist strategies for dealing with drought, it may consist in dispersal and reduction in herd size or transhumance to the south, to agricultural areas to exploit the available biomass (Mohamadou, 2004)

While the region's efforts have generated unmistakable improvements, adaptation projects are still often critiqued for focusing on hazards - such as drought - as opposed to addressing the underlying vulnerabilities which drive impacts (Epule, Chehbouni and Dhiba, 2021). As a way to target root causes, adaptive social protection programmes are increasingly being introduced throughout Sahel to strengthen the connections between social protection, disaster risk reduction, and climate change adaptation (Daron et al., 2020). Notable projects include *Sahel Adaptive Social Protection Programme (SASPP)* and *Adaptive Social Protection: Information for enhanced REsilience (ASPIRE)* which have reached millions of people and trained stakeholders on interpreting climate information as well as enabled seasonal forecasts for social protection decision-making purposes while strengthening the viability of anticipatory humanitarian action (Met Office, n.d.; Daron et al., 2020; World Bank, 2020).

Since 2020, EWEA programmes for drought, notably in the form of Forecast-based Financing (FbF), have increasingly been developed across the Sahel to reduce predictable impacts before they have had the chance to materialise. While both the United Nations Office for the Coordination of Humanitarian Affairs (OCHA) and Red Cross Society of Niger (RCSN) have established anticipatory mechanisms in Niger (OCHA, 2022a; IFRC, 2021), Chad is currently implementing a pilot (OCHA, 2022b). The selected early actions span the sectors of food security, livelihood, nutrition, protection, education, health, and WASH. When the drought conditions reached the predetermined threshold in April 2022, RCSN mobilised resources to replenish cereal bank reserves and roll out conditional cash transfers in Niger's worst affected region Zinder (IFRC, 2022). Long-term investments to address the region's chronic vulnerability are required, as this is what is driving the food crises, but scaling up anticipatory action programmes is an effective complement to reducing its impacts.

Part of these long-term investments could be into low-cost irrigation by pumping water from groundwater as the development of irrigated agriculture is one of the solutions for improving food security. A study in southwestern Niger shows that the groundwater, as a renewable resource, is better distributed in space than surface water (Nazoumou et al., 2016). The area's water and irrigable land resources have been located, quantified and their long-term potential re-evaluated on the basis of updated data. The results of the study show that 50,000 to 160,000 ha (three to nine percent of the total cultivated area) could be developed by small-scale irrigation from the most accessible groundwater (up to 20 metres deep) (Nazoumou et al., 2016). This estimate is of the same order of

magnitude as the one already made for surface water alone, thus doubling the irrigable potential of the area.

7.6 V&E Conclusions

Given the chronic food insecurity and vulnerable economic situation of many, even small shifts in rainfall (drought or floods) cascade and impact the already limited food supply in the Sahel. While not a focus on this study, high temperatures can also have a negative impact on crop production in West Africa. However, food security in the Sahel is dictated by a set of interrelated factors that go beyond climatic influences: violent conflict and insecurity, fragile states, increasing prices (due to a variety of globally-linked factors), a lack of development, poverty, and rain-dependent livelihoods.

Data availability

Almost all data are available via the Climate Explorer.

References

Beck, H. E., Vergopolan, N., Pan, M., Levizzani, V., van Dijk, A. I. J. M., Weedon, G. P., Brocca, L., Pappenberger, F., Huffman, G. J., and Wood, E. F.: Global-scale evaluation of 22 precipitation datasets using gauge observations and hydrological modeling, Hydrol. Earth Syst. Sci., 21, 6201–6217, https://doi.org/10.5194/hess-21-6201-2017, 2017.

Bombardi, R. J., Kinter, J. L., & Frauenfeld, O. W. (2019). A global gridded dataset of the characteristics of the rainy and dry seasons. Bulletin of the American Meteorological Society, 100(7), 1315-1328.

Beck, H. E., Wood, E. F., Pan, M., Fisher, C. K., Miralles, D. M., van Dijk, A. I. J. M., McVicar, T. R., and Adler, R. F. MSWEP V2 global 3‐hourly 0.1° precipitation: methodology and quantitative assessment *Bulletin of the American Meteorological Society* 100(3), 473–500, 2019

Ciavarella, A., Cotterill, D., Stott, P., Kew, S., Philip, S., van Oldenborgh, G. J., et al. (2021). Prolonged Siberian heat of 2020 almost impossible without human influence. *Climatic Change*, *166* (1), 9. https://doi.org/10.1007/s10584-021-03052-w

Eyring, V., Bony, S., Meehl, G. A., Senior, C. A., Stevens, B., Stouffer, R. J., and Taylor, K. E.: Overview of the Coupled Model Intercomparison Project Phase 6 (CMIP6) experimental design and organization, Geosci. Model Dev., 9, 1937–1958, https://doi.org/10.5194/gmd-9-1937-2016, 2016.

Famien, A. M., Janicot, S., Ochou, A. D., Vrac, M., Defrance, D., Sultan, B., and Noël, T.: A bias-corrected CMIP5 dataset for Africa using the CDF-t method – a contribution to agricultural impact studies, Earth Syst. Dynam., 9, 313–338, https://doi.org/10.5194/esd-9-313-2018, 2018.

Funk, C., Verdin, A., Michaelsen, J., Peterson, P., Pedreros, D., and Husak, G.: A global satellite-assisted precipitation climatology, Earth Syst. Sci. Data, 7, 275–287, https://doi.org/10.5194/essd-7-275-2015, 2015

Gaetani, M., Janicot, S., Vrac, M. *et al.* Robust assessment of the time of emergence of precipitation change in West Africa. *Sci Rep* **10**, 7670 (2020). https://doi.org/10.1038/s41598-020-63782-2

Hansen, J., Ruedy, R., Sato, M., & Lo, K. (2010). Global surface temperature change. Reviews of Geophysics, 48, RG4004. https://doi.org/10.1029/2010RG000345

E. Kriegler, N. Bauer, A. Popp, F. Humpenöder, M. Leimbach, J. Strefler, L. Baumstark, B. L. Bodirsky, J. Hilaire, D. Klein, I. Mouratiadou, I. Weindl, C. Bertram, J.-P. Dietrich, G. Luderer, M. Pehl, R. Pietzcker, F. Piontek, H. Lotze-Campen, A. Biewald, M. Bonsch, A. Giannousakis, U. Kreidenweis, C. Müller, S. Rolinski, A. Schultes, J. Schwanitz, M. Stevanovic, K. Calvin, J. Emmerling, S. Fujimori, and O. Edenhofer. Fossil-fueled development (ssp5): An energy and resource intensive scenario for the 21st century. Global Environmental Change, 42:297– 315, 2017. doi: https://doi.org/10.1016/j.gloenvcha.2016.05.015

Laux, H. Kunstmann, A. Bárdossy (2008) Predicting the regional onset of the rainy season in West Africa. Int. J. Climatol., 28 (2008), pp. 329-342, 10.1002/JOC.1542

LeBarbe L, Lebel T, Tapsoba D (2002) Rainfall variability in West Africa during the years 1950–90. J Climate 15:187–202

Lenssen, N., G. Schmidt, J. Hansen, M. Menne, A. Persin, R. Ruedy, and D. Zyss, 2019: Improvements in the uncertainty model in the Goddard Institute for Space Studies Surface Temperature (GISTEMP) analysis, J. Geophys. Res. Atmos., in press, doi:10.1029/2018JD029522.

Liebmann, B., and J. A. Marengo, 2001: Interannual variability of the rainy season and rainfall in the Brazilian Amazon basin. J. Climate, 14, 4308–4318, https://doi.org/10.1175/1520-0442(2001)014<4308: IVOTRS>2.0.CO;2

Maidment, Ross, Black, Emily and Young, Matthew (2017): TAMSAT Daily Rainfall Estimates (Version 3.0). University of Reading. Dataset. https://doi.org/10.17864/1947.112

Marteau, R., Sultan, B., Baron, C., Moron V., Traoré, S.B., and Alhassane, A. (2011) The onset of the rainy season and the farmer's sowing strategy for pearl millet cultivation in Southwest Niger, Agricultural and Forest Meteorology, doi:10.1016/j.agrformet.2011.05.018.

Philip, S., Kew, S., van Oldenborgh, G. J., Otto, F., Vautard, R., van der Wiel, K., et al. (2020). A protocol for probabilistic extreme event attribution analyses. Adv. Stat. Clim. Meteorol. Oceanogr., 6, 177–203, https://doi.org/10.5194/ascmo-6-177-2020, 2020.

K. Riahi, D. P. van Vuuren, E. Kriegler, J. Edmonds, B. C. O'Neill, S. Fujimori, N. Bauer, K. Calvin, R. Dellink, O. Fricko, W. Lutz, A. Popp, J. C. Cuaresma, S. Kc, M. Leimbach, L. Jiang, T. Kram, S. Rao, J. Emmerling, K. Ebi, T. Hasegawa, P. Havlik, F. Humpenöder, L. A. Da Silva, S. Smith, E. Stehfest, V. Bosetti, J. Eom, D. Gernaat, T. Masui, J. Rogelj, J. Strefler, L. Drouet, V. Krey, G. Luderer, M. Harmsen, K. Takahashi, L. Baumstark, J. C. Doelman, M. Kainuma, Z. Klimont, G. Marangoni, H. Lotze-Campen, M. Ober- steiner, A. Tabeau, and M. Tavoni. The Shared Socioeconomic Pathways and their energy, land use, and greenhouse gas emissions implications: An overview. Global Environmental Change, 42:153–168, Jan. 2017. ISSN 09593780. doi: 10.1016/j.gloenvcha.2016.05.009.

Sacré Regis M., D.; Mouhamed, L.; Kouakou, K.; Adeline, B.; Arona, D.; Houebagnon Saint. J., C.; Koffi Claude A., K.; Talnan Jean H., C.; Salomon, O.; Issiaka, S. Using the CHIRPS Dataset to Investigate Historical Changes in Precipitation Extremes in West Africa. *Climate* 2020, *8*, 84. https://doi.org/10.3390/cli8070084

F. Satgé, D. Defrance, B. Sultan, M.P. Bonnet, F. Seyler, N. Rouché, F. Pierron, J.E. Paturel. Evaluation of 23 gridded precipitation datasets across West Africa. J. Hydrol., 581 (2020), Article 124412, 10.1016/j.jhydrol.2019.124412

Sultan B., C. Baron, M. Dingkuhn, B. Saar et S. Janicot (2005). Agricultural impacts of large-scale variability of the West African monsoon, Agricultural and Forest Meteorology, 128 (1-2), 93-110.

Tarnavsky E., Grimes D., Maidment R., Black E., Allan R.P., Stringer M., Chadwick R., Kayitakire F. Extension of the TAMSAT satellite-based rainfall monitoring over Africa and from 1983 to present. J. Appl. Meteorol. Climatol., 53 (12) (2014), pp. 2805-2822

van Oldenborgh, G. J., van der Wiel, K., Kew, S., Philip, S., Otto, F., Vautard, R., et al. (2021). Pathways and pitfalls in extreme event attribution. *Climatic Change*, *166* (1), 13. https://doi.org/10.1007/s10584-021-03071-7

World Meteorological Organization WMO (2021). State of Climate Services: Risk Information and Early Warning Systems. WMO- No. 1252.

World Meteorological Organization WMO (2022). State of the Climate in Africa 2021. WMO- No. 1300.

Annex

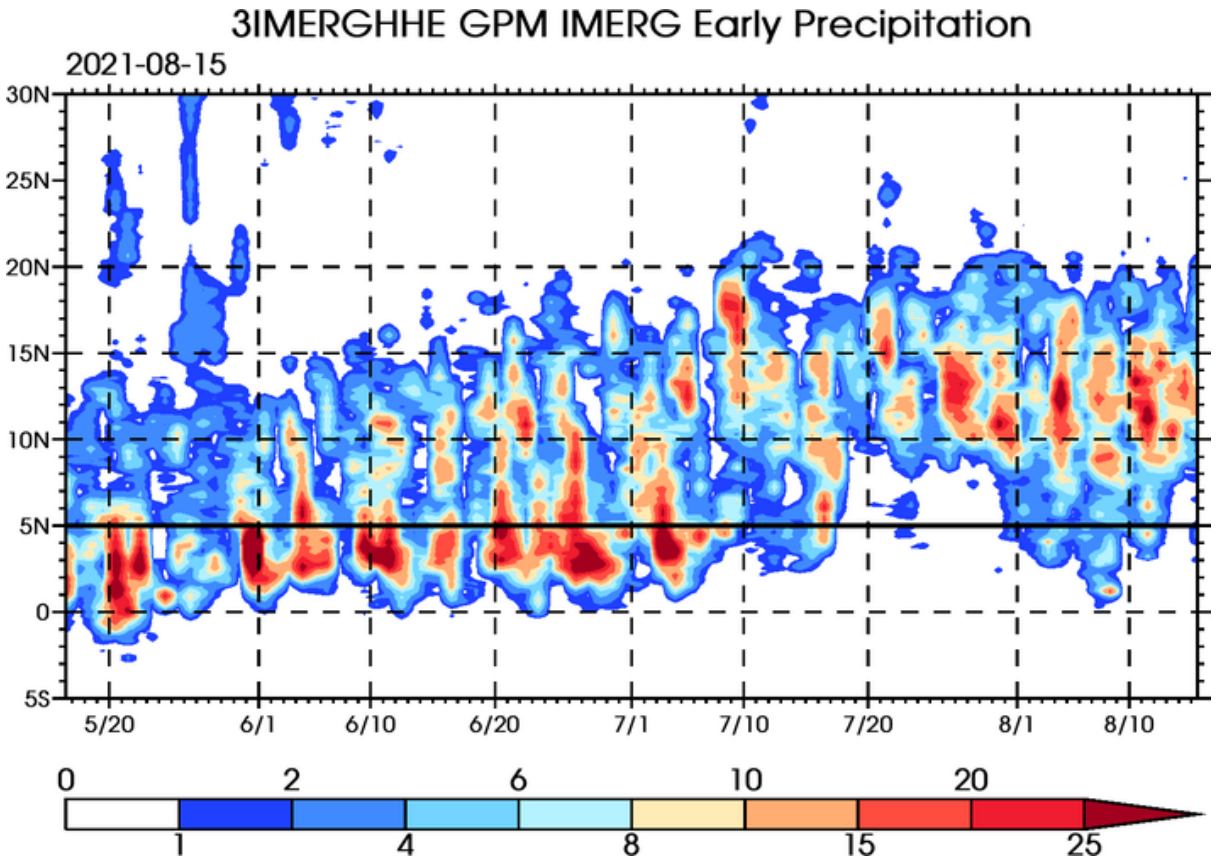
3IMERGHHE GPM IMERG Early Precipitation
2021-08-15
30N
25N
20N
15N
10N
5N
0
5S
5/20
6/1
6/10
6/20
7/1
7/10
7/20
8/1
8/10
0
2
6
10
20
1
4
8
15
25

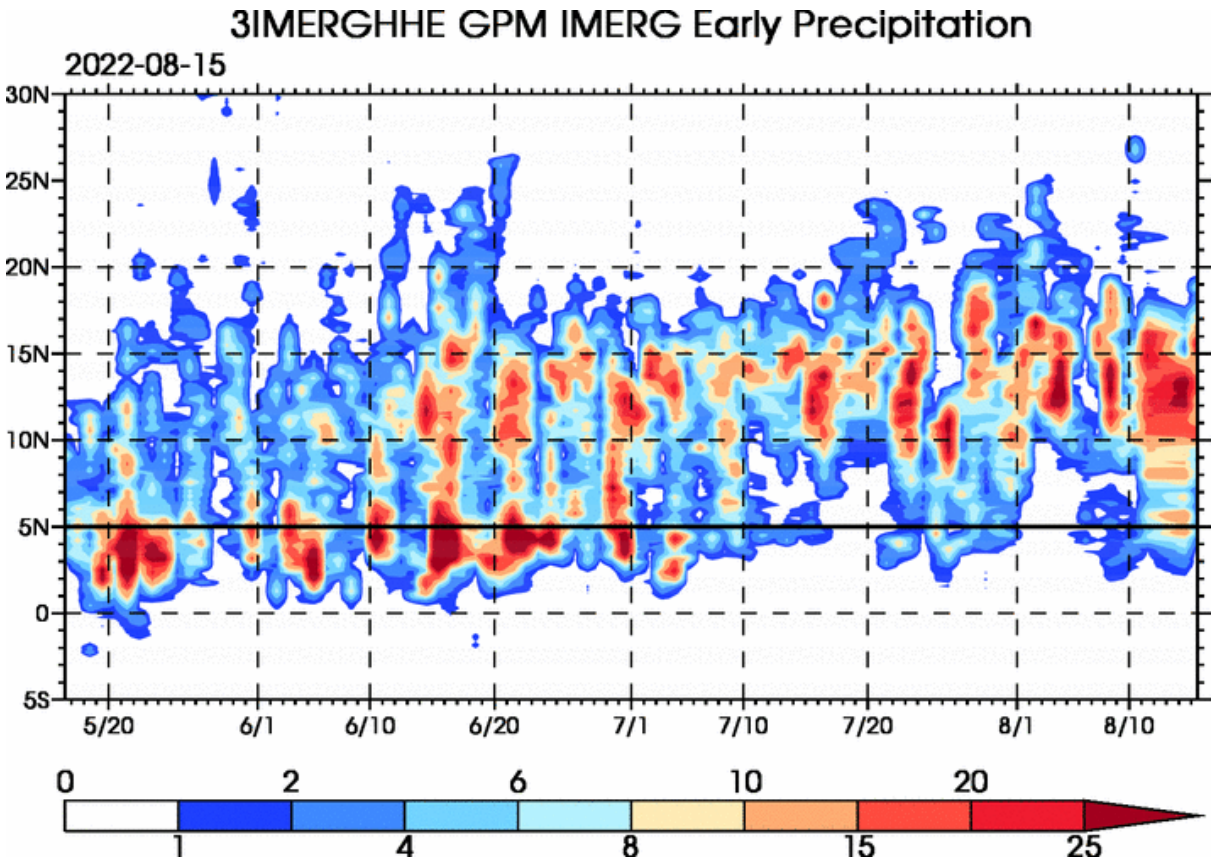

Annex Figure: Precipitation averaged [10W-10E] for 2021 and 2022 in unit mm/day: source: https://misva.aeris-data.fr/products/